JCI insight

Aging imparts cell-autonomous dysfunction to regulatory T cells during recovery from influenza pneumonia

Luisa Morales-Nebreda, … , Yuliya Politanska, Benjamin D. Singer

JCI Insight. 2021. https://doi.org/10.1172/jci.insight.141690.

Research In-Press Preview Aging

Graphical abstract

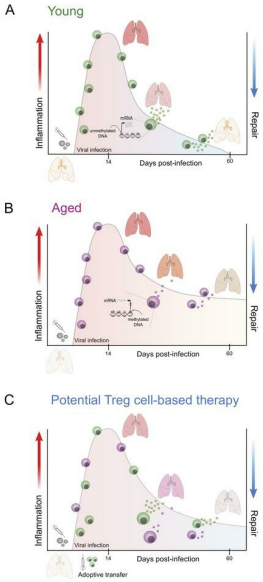

Aging imparts cell-autonomous dysfunction to regulatory T cells during recovery from influenza pneumonia

Luisa Morales-Nebreda[1], Kathryn A. Helmin[1], Manuel A. Torres Acosta[1], Nikolay S. Markov[1], Jennifer Yuan-Shih Hu[1], Anthony M. Joudi[1], Raul Piseaux-Aillon[1], Hiam Abdala-Valencia[1], Yuliya Politanska[1], Benjamin D. Singer[1,2,3*]

Author affiliations:
[1]Department of Medicine, Division of Pulmonary and Critical Care Medicine
Northwestern University Feinberg School of Medicine
Chicago, IL, 60611, USA

[2]Department of Biochemistry and Molecular Genetics
Northwestern University Feinberg School of Medicine
Chicago, IL, 60611, USA

[3]Simpson Querrey Institute for Epigenetics
Northwestern University Feinberg School of Medicine
Chicago, IL, 60611, USA

*To whom correspondence should be addressed:
Benjamin D. Singer, MD
Division of Pulmonary and Critical Care Medicine, Department of Medicine
Department of Biochemistry and Molecular Genetics
Simpson Querrey Institute for Epigenetics
Northwestern University Feinberg School of Medicine
Simpson Querrey, 5th Floor
Chicago, IL 60611 USA
benjamin-singer@northwestern.edu
Tel: (312) 503-4494
Fax: (312) 503-0411

Competing Interest Statement/Declaration of Interests
BDS has a pending patent application – US Patent App. 15/542,380, “Compositions and Methods to Accelerate Resolution of Acute Lung Inflammation.” The other authors declare no competing interests.

Abstract

Regulatory T (Treg) cells orchestrate resolution and repair of acute lung inflammation and injury following viral pneumonia. Compared with younger patients, older individuals experience impaired recovery and worse clinical outcomes after severe viral infections, including influenza and severe acute respiratory syndrome coronavirus 2 (SARS-CoV-2). Whether age is a key determinant of Treg cell pro-repair function following lung injury remains unknown. Here, we show that aging results in a cell-autonomous impairment of reparative Treg cell function following experimental influenza pneumonia. Transcriptional and DNA methylation profiling of sorted Treg cells provide insight into the mechanisms underlying their age-related dysfunction, with Treg cells from aged mice demonstrating both loss of reparative programs and gain of maladaptive programs. Novel strategies that restore youthful Treg cell functional programs could be leveraged as therapies to improve outcomes among older individuals with severe viral pneumonia.

Introduction

Age is the most important risk factor determining mortality and disease severity in patients infected with influenza virus or severe acute respiratory syndrome coronavirus 2 (SARS-CoV-2) (1-3). Global estimates of seasonal influenza-associated mortality range from 300,000-650,000 deaths per year, with the highest at-risk group comprised of individuals over age 75 (4). In the United States, influenza-associated morbidity and mortality have steadily increased, an observation linked to an expansion of the aging population. Pneumonia related to both severe influenza A virus and SARS-CoV-2 infection results in an initial acute exudative phase characterized by release of pro-inflammatory mediators that damage the alveolar epithelial and capillary barrier to cause refractory hypoxemia and the acute respiratory distress syndrome (ARDS) (5). If a patient survives this first stage, activation of resolution and repair programs during the ensuing recovery phase is crucial for restoration of lung architecture and function, which promotes liberation from mechanical ventilation, decreases intensive care unit length-of-stay and extends survival.

Immunomodulatory regulatory T (Treg) cells expressing the lineage-specifying transcription factor Foxp3 dampen inflammatory responses to both endogenous and exogenous antigens. Aside from their role in maintaining immune homeostasis through their capacity to suppress over-exuberant immune system activation, Treg cells reside in healthy tissues and accumulate in the lung in response to viral injury to promote tissue repair (6-8). Our group and others have shown that in murine models of lung injury, Treg cells are master orchestrators of recovery (9-12). Treg cells are capable of promoting tissue regeneration and repair, at least in part through release of reparative mediators such as the epidermal growth factor receptor ligand amphiregulin (Areg), which induces cell proliferation and differentiation of the injured tissue (13).

Epigenetic phenomena, including DNA methylation, modify the architecture of the genome to control gene expression and regulate cellular identity and function throughout the lifespan (14). Aside from being one of the best predictive biomarkers of chronological aging and age-related disease onset, DNA methylation regulates Treg cell identity through tight epigenetic control of *Foxp3* and Foxp3-dependent programs (15). Biological aging is associated with a progressive loss of molecular and cellular homeostatic mechanisms that maintain normal organ function, rendering individuals susceptible to disease (16, 17). Because of their tissue-reparative functions, Treg cells are important modulators of the immune response that promotes tissue regeneration following injury (18). Whether age plays a key role in determining the pro-repair function of Treg cells in the injured lung during recovery from viral pneumonia remains unknown. If aging indeed impacts Treg cell-mediated recovery, is it a Treg cell-autonomous phenomenon or is it because the aging lung microenvironment is resistant to Treg cell-mediated repair? Using heterochronic (age-mismatched) adoptive Treg cell transfer experiments and molecular profiling in mice, we sought to determine whether the age-related impairment in repair following influenza-induced lung injury is intrinsic to Treg cells. Our data support a paradigm in which aged Treg cells fail to upregulate youthful reparative programs, activate maladaptive responses and consequently exhibit a cell-autonomous impairment in pro-recovery function, which delays resolution from virus-induced lung injury among aged hosts.

Results

Aging results in increased susceptibility to influenza-induced lung injury due to impaired recovery

To evaluate the age-related susceptibility to influenza-induced lung injury, we administered influenza A/WSN/33 (H1N1) virus via the intratracheal route to young (2-4 months) and aged (18-22 months) wild-type mice. Aged mice exhibited > 50% mortality when compared with young animals (**Figure 1A**), impaired recovery of total body weight following a similar nadir (**Figure 1B**) and more severe lung injury by histopathology at a late recovery time point, day 60 post-infection (**Figure 1C**). At this same time point, aged mice also displayed an increase in the total number of cells per lung (**Figure 1D**), which were mainly comprised of immune cells identified by the pan-hematopoietic marker CD45 (**Figure 1E**), suggesting non-resolving tissue inflammation during recovery in older mice. Similar to prior reports (19, 20), we confirmed that the increased susceptibility to influenza-induced lung injury in aged mice is observed despite having cleared the virus at day 14 post-infection, the time of the greatest degree of weight loss among both groups (**Figure 1F**).

We next wanted to determine whether the age-related susceptibility to influenza-induced lung injury was due to a differential inflammatory response during the initial acute injury phase. Accordingly, we examined a different group of young and aged mice at a time point when viral clearance was complete and weight nadir was observed in both groups, 14 days post-infection. Aged mice demonstrated increased mortality when compared with young animals at this time point (**Supplemental Figure 1A**), but other markers of acute inflammation, including weight loss (**Supplemental Figure 1B**), total lung cells (**Supplemental Figure 1C**) and total lung $CD45^+$ cells in surviving animals were not significantly different between groups (**Supplemental Figure 1D**). Collectively, these results suggest that aging results in similar early injury but persistent lung inflammatory pathology during the recovery phase of influenza-induced lung injury.

Aging results in deficient repair following influenza-induced lung injury

Having established that aging results in an increased susceptibility to persistent lung inflammation and injury after influenza infection, we explored whether the impaired recovery in aged mice was linked to a persistent failure to repopulate the structural components of the alveolar-capillary barrier (i.e., failure to repair). Flow cytometry analysis (**Supplemental Figure 2**) of lung single-cell suspensions at day 60 post-influenza infection revealed an increased percentage of alveolar epithelial type 2 (AT2) cells ($CD45^-$, $T1\alpha^-$, $CD31^-$, $EpCAM^+/CD326^+$, $MHCII^+$) and endothelial cells ($CD45^-$, $T1\alpha^-$, $EpCAM^-/CD326^-$, $CD31^+$) (**Figure 2A-B** and **Figure 2D-E**, respectively) compared with the naïve state. Compared with young animals, aged mice post-influenza displayed a significantly lower total number of AT2 and endothelial cells (**Figure 2C** and **Figure 2F**, respectively).

In previous studies, investigators demonstrated that following influenza-induced lung injury, a population of cytokeratin 5^+ ($Krt5^+$) basal-like cells expand and migrate to the distal airspaces in an attempt to repair the injured epithelial barrier (21). These cells lack the capacity to transdifferentiate into functional AT2 cells, resulting in a dysplastic response that contributes to a dysregulated and incomplete repair phenotype following injury (22). Using a flow cytometry quantitative approach, we found that at 60 days post-infection, aged mice exhibited a significant increase in $Krt5^+$ cells compared with young animals (**Figure 2G-H**). In summary, older mice failed to repair the injured lung during the recovery phase of influenza-induced lung injury.

Aging determines the pro-recovery function of Treg cells following influenza-induced lung injury

We and others have identified an essential role for regulatory T (Treg) cells in orchestrating resolution and repair of acute lung injury (9-13). Having established that aged mice fail to repair the injured lung, we next sought to determine whether this finding is due to age-related features altering the lung microenvironment or is driven by cell-autonomous, age-associated Treg cell factors. Thus, we performed heterochronic (age-mismatched) adoptive transfer of $1x10^6$ splenic young or aged Treg cells (~90% $CD4^+CD25^{hi}Foxp3^+$, **Supplemental Figure 3A**) via retro-orbital injection into aged or young mice 24 hours post-influenza infection (**Figure 3A**). Notably, adoptive transfer of young Treg cells into aged hosts resulted in improved survival when compared with aged mice that received isochronic (age-aligned) adoptive transfer of aged Treg cells. Conversely, adoptive transfer of aged Treg cells into young hosts worsened their survival when compared with isochronic adoptive transfer of young Treg cells (**Figure 3B**).

To further characterize the effect of age on the splenic Treg cells used for adoptive transfer, we performed flow cytometry characterization of their Treg cell phenotype. In the spleen and other tissues, Treg cells can be phenotypically subdivided into resting or central Treg (cTreg) cells, which comprise the majority of the Treg cell pool in lymphoid organs, and activated or effector Treg (eTreg) cells which can migrate to non-lymphoid organs upon stimulation. Aged splenic Treg cells exhibited a significantly decreased percentage of cTreg cells and increased percentage of eTreg cells in both the naïve and post-influenza conditions (**Supplemental Figure 3B**). Additionally, to determine the rate of lung engraftment of splenic Treg cells following heterochronic adoptive transfer, we quantified the number of transferred splenic Treg cells in the lungs of recipient mice following influenza infection. Interestingly, we found a small but significant increase in the number of young Treg cells that engrafted into the lungs of aged mice when compared with aged Treg cells that were recovered from the lungs of young recipients (**Supplemental Figure 3C**).

We next turned to an inducible Treg cell depletion system using *Foxp3*^{DTR} mice in order to eliminate Treg cells from recipients and specifically determine the age-related effect of donor Treg cells on the susceptibility to influenza-induced lung injury (**Figure 3C**). Heterochronic adoptive transfer of aged Treg cells into Treg cell-depleted *Foxp3*^{DTR} mice 5 days post-infection resulted in increased mortality when compared with isochronic adoptive transfer of young Treg cells (**Figure 3D**). Combined, our findings demonstrate that the loss of Treg cell pro-repair function in aged hosts is dominated by intrinsic, age-related changes in Treg cells and not conferred extrinsically by the aging lung microenvironment.

Aging results in the loss of pro-repair transcriptional programs in Treg cells during recovery from influenza-induced lung injury

To further explore the mechanisms underpinning the age-related loss of Treg cell pro-repair function following influenza infection, we performed gene expression profiling using RNA-sequencing (RNA-seq) on flow cytometry sorted lung CD3ε^{+}CD4^{+}CD25^{hi}FR4^{+} Treg cells during the naïve state or late recovery phase from influenza (day 60 post-infection) (**Supplemental Figure 3D, Figure 4A**) (23). We confirmed that sorted lung CD3ε^{+}CD4^{+}CD25^{hi}FR4^{+} cells from both young and aged hosts express high levels of canonical Treg cell signature genes (*Foxp3, Il2ra, Il2rb, Nrp1, Ikzf2, Ctla4*) (**Supplemental Figure 3E**). Principal component analysis (PCA) of 3,132 differentially expressed genes (DEGs) after multiple group testing with false discovery rate (FDR) *q*-value < 0.05 demonstrated tight clustering by group assignment with PC1 reflecting the transcriptional response to influenza infection and PC2 reflecting age (**Figure 4B**). *K*-means clustering of these differentially expressed genes demonstrated that Cluster II was both the largest cluster and the one that defined the differential response to influenza infection between naïve and influenza-treated mice (**Figure 4C**). Notably, genes from this cluster were significantly upregulated among young Treg cells when compared with aged Treg cells following influenza

infection (**Figure 4D**). Functional enrichment analysis revealed that this cluster was enriched for processes related to tissue and vasculature development and extracellular matrix formation (see **Figure 4C**, right), suggesting an enhanced reparative phenotype of young compared with aged Treg cells.

We then performed an unsupervised analysis of the response to influenza infection from the naïve state to recovery phase between young and aged Treg cells. This analysis revealed upregulation of 1,174 genes ($\log_2$[fold-change] > 0.5, FDR *q*-value < 0.05) mostly linked to lung development (including epithelial and endothelial cell differentiation), extracellular matrix organization and wound healing (*Foxp2, Hhip, Klf2, Tns3, Hoxa5, Epcam, Erg, Bmper, Ereg, Lox, Tnc, Lama3* and *Spp1*) in young hosts (**Figure 5A-B**). We also found increased expression of genes associated with specialized Treg cell function in the maintenance of non-lymphoid tissue homeostasis and regenerative function (*Il1rl1* [encodes ST2, also known as IL33R]*, Il18r1*, *Il10* and *Areg*). Aged Treg cells demonstrated increased expression of cell cycle genes (*Kif15* and *Cdk1*), neutrophil chemotaxis (*Cxcr1, Cxcl1* and *S100a9*) and cytotoxic effector function (*Gmzk*). Gene set enrichment analysis (GSEA) of the pairwise comparison between young and aged Treg cells during the recovery phase following influenza infection revealed that aged Treg cells downregulated repair-associated processes such as epithelial-to-mesenchymal transition, myogenesis and angiogenesis when compared with young hosts (**Figure 6A-B**). This pairwise comparison demonstrated that while young Treg cells exhibited significantly increased expression of genes associated with naïve (resting) state and lymphoid tissue markers akin to central Treg (cTreg) cell phenotype (*Lef1, Sell, Satb1, Bcl2, S1pr1, Gpr83* and *Igfbp4*), aged Treg cells upregulated genes implicated in effector Th1, Th17 and Tfr differentiation (*Tbx21/Cxcr3, Hif-1a* and *Sostdc1,* respectively), cell cycle (*Ccna2, Mmc3* and *Msi2*), T cell anergy (*Rnf128*) and DNA damage response (*Xrcc5* and *Rm1*) (**Figure 6A**). Collectively, these results reveal that while young Treg cells display a reparative phenotype during the recovery phase from influenza

infection, aged Treg cells demonstrate both a less robust pro-repair phenotype when compared with young hosts and exhibit features of age-related maladaptive T cell responses, including effector T cell differentiation, cell cycle arrest and DNA damage responses (24).

Lung Treg cells from aged mice exhibit a less robust reparative response than lung Treg cells from young animals during recovery from influenza pneumonia

To further investigate the age-related reparative function of Treg cells during the recovery phase of influenza infection, we performed pairwise comparisons of both young and aged Treg cells from the naïve state and recovery phase (day 60 post-infection) (**Figure 7A and D**). We found that during the Treg cell response to influenza, there were 1,678 upregulated genes in young mice and only 445 upregulated genes in aged mice when compared with their respective naïve state (FDR q-value < 0.05). Gene set enrichment analysis revealed upregulation of pro-repair hallmark processes in both young and aged Treg cells during recovery from influenza infection (**Figure 7B-C and E-F**). We next compared the age-related transcriptional response to influenza infection and found 342 shared genes between both age groups that were associated with pro-repair processes (**Figure 8**). The remaining 1,336 uniquely upregulated genes in young Treg cells were linked to reparative processes in contrast with the 103 uniquely upregulated genes in aged Treg cells. Altogether, these results suggest that while aged Treg cells demonstrate a nominal reparative response during recovery from influenza infection, it is not as robust as the response exhibited by young Treg cells.

Previous studies have shown that Treg cells exhibiting a pro-repair phenotype express high levels of the alarmin IL-33 receptor (ST2), pro-inflammatory cytokine receptor IL-18 (IL18Rα or CD218α) and anti-inflammatory cytokine IL-10 (13, 25). We measured the protein expression of these molecules by flow cytometry and found similar expression between young and aged Treg cells 60 days post-influenza infection (**Supplemental Figure 4A**). We reasoned that measurement of only

three markers linked to repair incompletely characterizes the complexity of the Treg reparative landscape during influenza-induced lung injury and recovery. Accordingly, we compared our young and aged Treg cell RNA-seq dataset with previously published datasets describing reparative IL10$^+$ and IL18Rα$^+$ Treg cells (13). We found that reparative IL10$^+$ and IL18Rα$^+$ Treg cells were most similar to young Treg cells from our dataset when compared with aged Treg cells (**Supplemental Figure 4B**). Indeed, the number of genes within the unique intersections of young and IL10$^+$ and IL18Rα$^+$ Treg cells was significantly higher than the number of genes within the unique intersections of aged and IL10$^+$ and IL18Rα$^+$ Treg cells. Genes within the unique intersections of young and IL10$^+$ and IL18Rα$^+$ Treg cells were enriched for gene ontology (GO) processes linked to reparative processes including extracellular matrix remodeling, vascular remodeling and tube morphogenesis (**Supplemental Figure 4B**). These results underscore our finding that the youthful Treg cell response during recovery from influenza pneumonia is defined by a more robust reparative phenotype when compared with aged hosts.

Regulatory T cells from aged mice demonstrate a pro-inflammatory effector phenotype during recovery from influenza pneumonia

Upon stimulation, Treg cells can exhibit phenotypic and functional adaptability through upregulation of transcription factors and chemokine receptors akin to effector T helper cell subsets (e.g., Th1, Th2, Th17 and T follicular regulatory or Tfr) (26). The resulting eTreg cells with Th-like phenotypes migrate to inflammatory non-lymphoid tissues and acquire transcriptional and functional programs that copy the T effector responses they intend to suppress (27, 28). Having observed transcriptional upregulation of effector-associated factors in the aged Treg cell response during recovery from influenza infection, we next performed flow cytometry analysis to measure canonical effector-associated transcription factors and cytokines at the protein level. During the recovery phase following influenza infection, aged mice exhibited a higher percentage of eTreg cells in their lungs when compared with young hosts (**Figure 9A**). In the lung, when compared

with young $CD4^+Foxp3^+$ cells, aged cells exhibited significantly higher expression of the transcription factors Tbet and Ror-γt, canonical master regulators of Th1 and Th17 responses, respectively (**Figure 9B**). Surprisingly, intracellular cytokine profiling of these cells also demonstrated a significant increase in the percentage of Ifn-γ- and IL-17-producing $CD4^+Foxp3^+$ cells in the lungs of aged mice when compared with young mice (**Figure 9C**).

Profiling of multiple well-established Treg cell suppressive markers, including *Foxp3*, showed no significant age-related difference during the recovery phase of influenza infection (**Supplemental Figure 5A**). In addition, aged and young Treg cells exhibited similar suppressive function in vitro, although there was a trend toward increased suppressive function in aged cells as has been suggested by a previous report (**Supplemental Figure 5B**) (29). These data suggest that Treg cells in the lungs of aged animals upregulate inflammatory effector programs during recovery from influenza. While these effector programs are ostensibly protective during acute influenza-induced acute lung injury, they may represent an age-related maladaptive Treg cell response leading to unremitting lung inflammation and injury during recovery.

DNA methylation regulates the transcriptional pro-repair response to influenza infection

In addition to representing one of the hallmarks of aging, epigenetic phenomena such as DNA methylation regulate the development, differentiation and functional specialization of T cell lineages, including Treg cells (14-16, 30). Therefore, we reasoned that age-related changes to the Treg cell DNA methylome could inform the divergent pro-repair transcriptional response observed between young and aged Treg cells following influenza infection. We performed genome-wide (5'-cytosine–phosphate–guanine-3') CpG methylation profiling with modified reduced representation bisulfite sequencing (mRRBS) of sorted lung Treg cells during the naïve state or recovery phase following influenza infection (day 60) (**Figure 10A**). PCA of ~70,000

differentially methylated cytosines (DMCs, FDR *q*-value < 0.05) revealed tight clustering according to group assignment with the main variance across the dataset (PC1) reflecting methylation changes due to age (**Figure 10B**), consistent with prior studies (17, 31). We next identified genes that were both differentially expressed and contained differentially methylated cytosines within their gene promoters (ANOVA, FDR *q*-value <0.05), finding 1,319 genes meeting this strict parameter threshold (**Figure 10C**). *K*-means clustering of these genes' expression levels revealed similarity to the overall DEG heat map in Figure 4C, suggesting a strong correlation between differential DNA methylation and transcription. Gene set enrichment analysis of these genes demonstrated that this methylation-regulated gene expression program was associated with pro-recovery processes and was significantly skewed toward young Treg cells (**Figure 10C**). Combined, these results support that age-related DNA methylation regulates the reparative transcriptional regulatory network during recovery from influenza-induced lung injury.

Discussion

We sought to unambiguously address the paradigm of how aging affects Treg cell function during recovery from influenza pneumonia. We used heterochronic (age-mismatched) Treg cell adoptive transfer following influenza infection to establish that the age-related pro-repair function of these cells is determined by cell-autonomous mechanisms. While adoptive transfer of young Treg cells into aged or Treg-cell depleted hosts demonstrated a salutary effect, the transfer of aged cells into young or Treg-cell depleted hosts had a detrimental impact on mortality. Comprehensive transcriptional and DNA methylation profiling revealed age-related epigenetic repression of the youthful reparative gene expression profile and activation of maladaptive responses in lung Treg cells among aged hosts.

The ongoing coronavirus disease 19 (COVID-19) pandemic caused by severe acute respiratory syndrome coronavirus 2 (SARS-CoV-2) represents an unprecedented challenge for the scientific community to identify novel pharmacotherapies and strategies for effective disease management. Most studies have addressed the early mechanistic events leading to viral pneumonia-induced lung injury yet failed to develop efficacious therapies to improve outcomes among patients with viral ARDS. Thus, we focused our experimental design on the late stages of recovery from influenza infection with the goal of investigating novel reparative pathways that could be leveraged to enhance lung resilience to viral pneumonia in older hosts. Both influenza A virus- and SARS-CoV-2-induced lung injury disproportionately affect the elderly, who comprise the greatest proportion of infection-related deaths (1, 3, 32, 33). Here, we found that similar to human epidemiologic data and previous pre-clinical murine studies, aged mice exhibit increased susceptibility and impaired recovery following influenza infection (4, 19). Injury to alveolar epithelial type I, II and endothelial cells disrupts the tight gas exchange barrier causing accumulation of fluid and pro-inflammatory mediators in the alveolar space, a hallmark of ARDS pathophysiology (5). Notably, we found that during late recovery from influenza infection, aged

hosts demonstrated a decreased number of alveolar epithelial type II cells and endothelial cells when compared with young animals, suggesting that failure to repopulate the alveolar lining contributes to the observed age-related impairment in recovery. Severe influenza infection leads to a robust expansion of $Krt5^+$ cells, which migrate distally to form cystic-like structures or pods intended to cover the damaged alveolar wall (22). These pods persist long after the initial infection, lack the capacity to generate a functional alveolar epithelium and therefore constitute an insufficient reparative response to injury (22). Here, we found that aged animals display an increased percentage of $Krt5^+$ cells during the recovery phase of influenza-induced lung injury, which reflects the dysregulated repair response among aged hosts.

Over the past decade, regulatory T cells have emerged as key mediators of wound healing and tissue regeneration (7, 18, 34). This group of specialized cells has been primarily known for their ability to suppress effector immune cell subsets leading to resolution of inflammation, but they are also capable of directly affecting tissue regeneration through production of pro-repair mediators such as amphiregulin and keratinocyte growth factor (13, 25, 35). Investigators have demonstrated that aging can negatively impact the composition and function of the Treg cell pool throughout the lifespan, rendering them inefficient as mediators of tissue repair (36). This decline might occur through cell-autonomous mechanisms resulting in altered trafficking to the lung and T cell maladaptive responses that lead to increased susceptibility to disease. For instance, loss of stemness accompanied by differentiation into pro-inflammatory Th1/Th17 phenotypes, activation of DNA damage responses and the senescence secretome are among some of the T cell maladaptations that result from the mounting challenges to which the T cell repertoire is exposed over a lifetime (24). These T cell maladaptive changes could also result from an age-related decline in stromal signals and circulating factors from the tissue microenvironment that either affect T cell function directly or render the microenvironment resistant to T cell responses. Our heterochronic adoptive Treg cell transfer experiments definitively address this paradigm,

ascertaining that the observed age-related Treg cell dysfunction is due to cell-autonomous mechanisms and dominant over the aged pulmonary microenvironment. Our data demonstrate that aging not only imparts a loss of pro-recovery Treg cell function but also a gain of some of these maladaptive features when compared with young hosts. Future studies should aim to address the respective contribution of loss-of-reparative or gain-of-maladaptive function to the overall phenotype and function of aged Treg cells during viral-induced lung injury and recovery.

What are the molecular mechanisms underpinning the age-associated Treg cell loss-of reparative function in the lung following influenza infection? Gene expression profiling of lung Treg cells during the recovery phase of influenza infection revealed that young Treg cells significantly upregulated genes (when compared with aged Treg cells) linked to biologic processes associated with a robust pro-repair signature, including extracellular matrix organization, alveologenesis and vasculogenesis. Here, we demonstrate that the young Treg cell pro-repair program is dominated by *Areg* expression and other genes related to the above-mentioned reparative processes. Interestingly, we found no difference when comparing the suppressive phenotype and function of young versus aged Treg cells following influenza infection and during steady state. These results suggest that the reparative program of Treg cells is separable and distinct from their suppressive program, an important observation that informs the development of novel Treg cell-based immunotherapies to target molecular pathways regulating their reparative function. In regard to aged Treg cells, we found that although capable of upregulating a pro-repair program following influenza infection, it is far less robust when compared with the youthful reparative response. Moreover, aged Treg cells displayed increased expression of genes associated with an effector phenotype with increased expression of canonical Th1 and Th17 lineage markers (Tbet/Ifn-γ and Ror-γt/IL-17, respectively). Whether this finding represents an age-related functional adaptability

of Treg cells following influenza infection or it is the result of Treg cell lineage instability leading to effector differentiation remains unknown.

For our studies, due to the practical limitations of aging *Foxp3* genetic reporter animals, we identified Treg cells as $CD3\varepsilon^{+}CD4^{+}CD25^{hi}FR4^{+}$, a strategy validated by our transcriptomics data (**Supplemental Figure 3E**) and previous work (23). Nevertheless, bulk RNA-seq analysis averages gene expression profiles across a heterotypic Treg cell pool and presents them as a monotypic population, constituting a limitation to our data interpretation. Future studies should implement single-cell technologies to accurately describe the heterogeneity of the Treg cell landscape during virus-induced lung injury and recovery, which will allow investigators to identify Treg subpopulations that can be leveraged for cell-based therapies.

Establishment of a Treg cell-specific DNA methylation pattern at key genomic loci is necessary to maintain the lineage stability and immunosuppressive function of Treg cells (15, 30). Epigenomic profiling has revealed that Treg cell-specific alterations in methylation patterning modulate Treg cell transcriptional programs and increase susceptibility to human autoimmune diseases (37). Whether epigenetic phenomena have a similar regulatory role in modulating the Treg cell reparative gene expression program remains unknown. Here, we used an unsupervised bioinformatics analysis to uncover a Treg cell-specific methylation-regulated transcriptional program enriched for reparative processes during recovery from influenza infection. Our computational integrative approach provides inferential evidence that age-related DNA methylation can modify the expression of genes linked to pro-repair processes in Treg cells but does not prove causality and therefore represents a limitation of our study. Future research could focus on leveraging epigenome editing technologies to establish the causality of age-related, Treg cell-specific DNA methylation patterns in controlling their regenerative function (38).

In conclusion, our study establishes that aging imparts cell-autonomous dysfunction to the reparative capacity of Treg cells following influenza pneumonia. The youthful reparative transcriptional response of Treg cells is dominated by processes linked to epithelial and endothelial cell repair and extracellular matrix remodeling and demonstrates regulation by DNA methylation. Aged Treg cells exhibited a less robust reparative program and displayed features of maladaptive T cell responses. These findings carry important implications for the development of small molecule- and Treg cell-based therapeutics that promote restoration of lung architecture and function following viral pneumonia in our increasingly older population.

Methods

Mice

Young (2-4-month-old) and aged (18-22-month-old) C57BL/6 mice were obtained from NIA Aged Rodent Colony. *Foxp3*^{DTR} mice were purchased from The Jackson Laboratory (Jax 016958). Animals received water *ad libitum*, were housed at a temperature range of 20-23 °C under 14/10-hour light/dark cycles, and received standard rodent chow.

Administration of influenza A virus and lung histopathology

Wild-type C57BL/6 mice were anesthetized with isoflurane and intubated using a 20-gauge angiocatheter cut to a length that placed the tip of the catheter above the carina. Mice were instilled with a mouse-adapted influenza A virus (A/WSN/33 [H1N1]) (3 pfu/mouse or 2 pfu/mouse for *Foxp3*^{DTR} mice, in 50 µL of sterile PBS) as previously described (39).

To prepare organ tissues for histopathology, the inferior vena cava was cut and the right ventricle was perfused *in situ* with 10 mL of sterile PBS. A 20-gauge angiocatheter was then sutured into the trachea via a tracheostomy. The lungs were removed *en bloc* and inflated to 15 cm H_2O with 4% paraformaldehyde. 5-µm sections from paraffin-embedded lungs were stained with hematoxylin-eosin and examined using light microscopy with a high-throughput, automated, slide imaging system, TissueGnostics (TissueGnostics GmbH).

Tissue preparation, flow cytometry analysis and sorting

Single-cell suspensions from harvested mouse lungs were prepared and stained for flow cytometry analysis and flow cytometry sorting as previously described using the reagents listed in **Supplemental Table 1** (15, 40, 41). The $CD4^+$ T Cell Isolation Kit, mouse (Miltenyi) was used to enrich $CD4^+$ T cells in single-cell suspensions prior to flow cytometry sorting. Cell counts of single-cell suspensions were obtained using a Cellometer with AO/PI staining (Nexcelom

Bioscience) before preparation for flow cytometry. Data acquisition for analysis was performed using a BD Symphony A5 instrument with FACSDiva software (BD). Cell sorting was performed using the 4-way purity setting on BD FACSAria SORP instruments with FACSDiva software. Analysis was performed with FlowJo v10.6.1 software.

Cytokine measurements

Lungs were harvested from young and aged mice and a single-cell suspension was obtained. Red blood cells were removed with ACK Lysis Buffer (Thermo Fisher) following the manufacturer's instructions. Single-cell suspensions were plated on 12-well cell culture plates (Thermo Fisher) at a concentration of 1 x 10^6 cells/mL with RPMI plus 2 µL/mL Leukocyte Activation Cocktail with GolgiPlug (BD) and incubated for 4 hours at 37 °C. After incubation, cells were resuspended in PBS and stained with a viability dye and subsequently with fluorochrome-conjugated antibodies directed at IFN-γ (clone XMG1.2), IL-17 (clone TC11-18H1), IL-10 (clone JES5-16E3) and IL-4 (clone 11B11). Data acquisition and analysis was performed as described above.

Treg cell isolation and adoptive transfer

Splenic $CD4^+CD25^+$ Treg cells were isolated from euthanized young (2-4-month-old) and aged (18-22-month-old) C57BL/6 mice by use of magnetic separation with the EasySep™ Mouse $CD4^+CD25^+$ Regulatory T Cell Isolation Kit II (STEMCELL Technologies) according to the manufacturer's instructions. A separate group of young and aged C57BL/6 mice were challenged with 3 pfu/mouse of influenza A virus as previously described (39). Twenty-four hours later a single-cell suspension of isolated 1 x 10^6 splenic Treg cells in 100 µL of sterile PBS was obtained and transferred via retro-orbital injection into the influenza-treated mice. *Foxp3*^{DTR} mice were challenged with 2 pfu/mouse of influenza A virus. Diphtheria toxin (List Biologicals, CA) was

administered via intraperitoneal injection in 100 μL of sterile PBS in the following doses and days relative to influenza A virus infection (day 0): 50 mcg/kg on day -2 and 10 mcg/kg every 48 hours starting on day 0 and ending on day 28 post-infection. Five days later, 1 x 10^6 young or aged splenic Treg cells in 100 μL of sterile PBS were transferred via retro-orbital injection into the influenza-treated *Foxp3*^{DTR} mice.

RNA-sequencing

Flow cytometry sorted lung Treg cells were pelleted in RLT plus buffer with 1% 2-mercaptoethanol and stored at -80 °C until RNA extraction was performed. The Qiagen AllPrep DNA/RNA Micro Kit was used for simultaneous isolation of RNA and DNA (15, 42). RNA quality was assessed using a 4200 TapeStation System (Agilent Technologies). mRNA was isolated from purified 1 ng total RNA using oligo-dT beads (New England Biolabs, Inc). The NEBNext Ultra™ RNA kit was used for full-length cDNA synthesis and library preparation. Libraries were pooled, denatured and diluted, resulting in a 2.0 pM DNA solution. PhiX control was spiked in at 1%. Libraries were sequenced on an Illumina NextSeq 500 instrument (Illumina) using the NextSeq 500 High Output reagent kit (1x75 cycles). For RNA-seq analysis, FASTQ reads were demultiplexed with bcl2fastq v2.17.1.14, trimmed with Trimmomatic v0.38 (to remove low quality basecalls), and aligned to the *Mus musculus* or mm10 (GRCm38) reference genome using TopHat v.2.1.0. Resultant bam files were imported into SeqMonk v1.45.4 to generate raw counts tables with the RNA-seq quantitation pipeline and filtered by protein-coding genes. Annotated probe reports from SeqMonk were imported into RStudio for downstream analysis. Differential gene expression analysis was performed with the edgeR v3.28.1 R/Bioconductor package using R v3.6.3 and RStudio v1.2.1578 (43). A genomic dataset visualization tool, Morpheus web interface (https://software.broadinstitute.org/morpheus/), was used to perform *K*-means clustering and heat maps. Gene ontology analysis was performed by using either the Molecular Signatures Database

(MSigDB) from The Broad Institute or the Metascape interface. Gene Set Enrichment Analysis was performed using the Broad Institute's GSEA v4.0.3 software with the GSEAPreranked tool. A ranked gene list from young and aged phenotypes was ordered by $\log_2$(fold-change) in average expression, using 1,000 permutations and the Hallmark Gene Set database (44).

Modified reduced representation bisulfite sequencing

Genomic DNA was isolated from sorted lung Treg cells using Qiagen AllPrep DNA/RNA Micro Kit. Endonuclease digestion, fragment size selection, bisulfite conversion and library preparation were performed as previously described (15, 43, 45-47). Sequencing was performed on a NextSeq 500 instrument (Illumina). DNA methylation analysis and quantification were performed using Trim Galore! v0.4.3, Bismark v0.16.3, DSS v2.30.1 R/Bioconductor package and the bisulphite feature methylation pipeline from the SeqMonk platform. *Mus musculus* or mm10 (GRCm38) was used as the reference genome.

Lymphocyte suppression assay

In vitro Treg cell suppression assays were performed as previously described (9, 48). In brief, splenic $CD4^+CD25^+$ cells (~90% $Foxp3^+$) were isolated using the EasySep™ Mouse $CD4^+CD25^+$ Regulatory T Cell Isolation Kit II (STEMCELL Technologies), incubated with a 1:1 ratio of anti-CD3/CD28-coated MACSiBeads (Miltenyi Biotech) and co-cultured with differing ratios of Treg to CellTrace Violet (Thermo Fisher) -labeled $CD4^+$ T effector (Teff) cells, which were obtained from 8-week-old wild-type mice. After 48 hours, effector T cell proliferation was assayed by flow cytometry analysis.

Viral plaque assay

Viral plaque assays were performed as we previously described (49). In brief, MDCK cells were cultured in 6-well plates and grown to 100% confluence. Lung homogenates were obtained from

mice at 14 days post-infection. MDCK cells were incubated with serial dilutions of lung homogenates or control influenza A virus in DMEM plus 1% bovine serum albumin (BSA) at 37°C for 2 hours. Replacement media (4 mL/well) composed of DMEM, autoclaved Avicel 2.4% and N-acetyl-trypsin was added and incubated for 3 days. The media was subsequently removed and plaques were visualized with blue-black staining (0.1% naphthalene black, 6% glacial acetic acid and 13.6% anhydrous sodium acetate) (49).

Statistical analysis

All statistical tests are detailed either in the Results section or figure legends. Statistical analysis was performed using either GraphPad Prism v8.3.0 or R v3.6.3. Computational analysis was performed using Genomics Nodes and Analytics Nodes on Quest, Northwestern University's High-Performance Computing Cluster.

Data and material availability

The raw and processed next-generation sequencing data sets have been uploaded to the GEO database (https://www.ncbi.nlm.nih.gov/geo/) under accession number GSE151543. Code used for analysis of **Supplemental Figure 4B** is available at https://github.com/NUPulmonary/2020_MoralesNebreda.

Study approval

All animal experiments and procedures were conducted in accordance with the standards established by the United States Animal Welfare Act set forth in National Institutes of Health guidelines and were approved by the Institutional Animal Care and Use Committee (IACUC) at Northwestern University under protocols IS00006605 and IS00012955.

Author contributions

LMN and BDS contributed to the conception, hypothesis delineation and design of the study; LMN, KAH, MATA, NSM, JY-SH, AMJ, RP-A, HA-V, YP and BDS performed experiments/data acquisition and analysis. LMN and BDS wrote the manuscript.

Acknowledgements

We thank the Northwestern University Flow Cytometry Core Facility supported by Cancer Center Support Grant (NCI CA060553). Flow cytometry Cell Sorting was performed using BD FACSAria SORP systems purchased through the support of NIH 1S10OD011996-01 and 1S10OD026815-01. Histology services were provided by the Northwestern University Mouse Histology and Phenotyping Laboratory, which is supported by P30CA060553 awarded to the Robert H. Lurie Comprehensive Cancer Center. Imaging work was performed at the Northwestern University Center for Advanced Microscopy generously supported by NCI CCSG P30CA060553 awarded to the Robert H. Lurie Comprehensive Cancer Center. We also wish to thank the Northwestern University RNA-Sequencing Center/Genomics Lab of the Pulmonary and Critical Care Medicine and Rheumatology Divisions. This research was supported in part through the computational resources and staff contributions provided by the Genomics Compute Cluster, which is jointly supported by the Feinberg School of Medicine, the Center for Genetic Medicine, and Feinberg's Department of Biochemistry and Molecular Genetics, the Office of the Provost, the Office for Research, and Northwestern Information Technology. The Genomics Compute Cluster is part of Quest, Northwestern University's high-performance computing facility, with the purpose to advance research in genomics.

Funding

LMN was supported by NIH awards T32HL076139 and F32HL151127. MATA was supported by NIH award T32GM008152. BDS was supported by NIH awards K08HL128867, U19AI135964, P01AG049665 and R01HL149883 and the Eleanor Wood Prince Grant of the Woman's Board of Northwestern Memorial Hospital.

References

1. Thompson WW, Comanor L, and Shay DK. Epidemiology of seasonal influenza: use of surveillance data and statistical models to estimate the burden of disease. *J Infect Dis.* 2006;194 Suppl 2:S82-91.

2. Liu Y, Mao B, Liang S, Yang JW, Lu HW, Chai YH, et al. Association between age and clinical characteristics and outcomes of COVID-19. *Eur Respir J.* 2020;55(5):2001112.

3. Torres Acosta MA, and Singer BD. Pathogenesis of COVID-19-induced ARDS: implications for an aging population. *European Respiratory Journal.* 2020:2002049.

4. Iuliano AD, Roguski KM, Chang HH, Muscatello DJ, Palekar R, Tempia S, et al. Estimates of global seasonal influenza-associated respiratory mortality: a modelling study. *The Lancet.* 2018;391(10127):1285-300.

5. Matthay MA, Zemans RL, Zimmerman GA, Arabi YM, Beitler JR, Mercat A, et al. Acute respiratory distress syndrome. *Nat Rev Dis Primers.* 2019;5(1):18.

6. Walter JM, Helmin KA, Abdala-Valencia H, Wunderink RG, and Singer BD. Multidimensional assessment of alveolar T cells in critically ill patients. *JCI Insight.* 2018;3(17).

7. Li J, Tan J, Martino MM, and Lui KO. Regulatory T-Cells: Potential Regulator of Tissue Repair and Regeneration. *Frontiers in Immunology.* 2018;9(585).

8. Grant RA, Morales-Nebreda L, Markov NS, Swaminathan S, Querrey M, Guzman ER, et al. Circuits between infected macrophages and T cells in SARS-CoV-2 pneumonia. *Nature.* 2021.

9. Singer BD, Mock JR, Aggarwal NR, Garibaldi BT, Sidhaye VK, Florez MA, et al. Regulatory T cell DNA methyltransferase inhibition accelerates resolution of lung inflammation. *Am J Respir Cell Mol Biol.* 2015;52(5):641-52.

10. D'Alessio FR, Tsushima K, Aggarwal NR, West EE, Willett MH, Britos MF, et al. CD4+CD25+Foxp3+ Tregs resolve experimental lung injury in mice and are present in humans with acute lung injury. *The Journal of Clinical Investigation.* 2009;119(10):2898-913.

11. Mock JR, Dial CF, Tune MK, Norton DL, Martin JR, Gomez JC, et al. Transcriptional analysis of Foxp3+ Tregs and functions of two identified molecules during resolution of ALI. *JCI Insight.* 2019;4(6).

12. Garibaldi BT, D'Alessio FR, Mock JR, Files DC, Chau E, Eto Y, et al. Regulatory T cells reduce acute lung injury fibroproliferation by decreasing fibrocyte recruitment. *Am J Respir Cell Mol Biol.* 2013;48(1):35-43.

13. Arpaia N, Green JA, Moltedo B, Arvey A, Hemmers S, Yuan S, et al. A Distinct Function of Regulatory T Cells in Tissue Protection. *Cell.* 2015;162(5):1078-89.

14. Morales-Nebreda L, McLafferty FS, and Singer BD. DNA methylation as a transcriptional regulator of the immune system. *Translational research : the journal of laboratory and clinical medicine.* 2019;204:1-18.

15. Helmin KA, Morales-Nebreda L, Acosta MAT, Anekalla KR, Chen S-Y, Abdala-Valencia H, et al. Maintenance DNA methylation is essential for regulatory T cell development and stability of suppressive function. *The Journal of Clinical Investigation.* 2020;130(12):6571-87.

16. Khan SS, Singer BD, and Vaughan DE. Molecular and physiological manifestations and measurement of aging in humans. *Aging Cell.* 2017;16(4):624-33.

17. Horvath S, and Raj K. DNA methylation-based biomarkers and the epigenetic clock theory of ageing. *Nat Rev Genet.* 2018;19(6):371-84.

18. Singer BD, and Chandel NS. Immunometabolism of pro-repair cells. *J Clin Invest.* 2019;129(7):2597-607.

19. Goplen NP, Wu Y, Son YM, Li C, Wang Z, Cheon IS, et al. Tissue-resident CD8 T cells drive age-associated chronic lung sequelae after viral pneumonia. *Science Immunology.* 2020;5(53):eabc4557.

20. Lanzer KG, Cookenham T, Reiley WW, and Blackman MA. Correction to: Virtual memory cells make a major contribution to the response of aged influenza-naïve mice to influenza virus infection. *Immunity & Ageing.* 2018;15(1):18.

21. Vaughan AE, Brumwell AN, Xi Y, Gotts JE, Brownfield DG, Treutlein B, et al. Lineage-negative progenitors mobilize to regenerate lung epithelium after major injury. *Nature.* 2015;517(7536):621-5.

22. Kanegai CM, Xi Y, Donne ML, Gotts JE, Driver IH, Amidzic G, et al. Persistent Pathology in Influenza-Infected Mouse Lungs. *Am J Respir Cell Mol Biol.* 2016;55(4):613-5.

23. Yamaguchi T, Hirota K, Nagahama K, Ohkawa K, Takahashi T, Nomura T, et al. Control of immune responses by antigen-specific regulatory T cells expressing the folate receptor. *Immunity.* 2007;27(1):145-59.

24. Goronzy JJ, and Weyand CM. Successful and Maladaptive T Cell Aging. *Immunity.* 2017;46(3):364-78.

25. Burzyn D, Kuswanto W, Kolodin D, Shadrach JL, Cerletti M, Jang Y, et al. A special population of regulatory T cells potentiates muscle repair. *Cell.* 2013;155(6):1282-95.

26. Josefowicz SZ, Lu L-F, and Rudensky AY. Regulatory T cells: mechanisms of differentiation and function. *Annu Rev Immunol.* 2012;30:531-64.

27. Miragaia RJ, Gomes T, Chomka A, Jardine L, Riedel A, Hegazy AN, et al. Single-Cell Transcriptomics of Regulatory T Cells Reveals Trajectories of Tissue Adaptation. *Immunity.* 2019;50(2):493-504 e7.

28. Burzyn D, Benoist C, and Mathis D. Regulatory T cells in nonlymphoid tissues. *Nat Immunol.* 2013;14(10):1007-13.

29. Garg SK, Delaney C, Toubai T, Ghosh A, Reddy P, Banerjee R, et al. Aging is associated with increased regulatory T-cell function. *Aging Cell.* 2014;13(3):441-8.

30. Ohkura N, Hamaguchi M, Morikawa H, Sugimura K, Tanaka A, Ito Y, et al. T cell receptor stimulation-induced epigenetic changes and Foxp3 expression are independent and complementary events required for Treg cell development. *Immunity.* 2012;37(5):785-99.

31. Chen BH, Marioni RE, Colicino E, Peters MJ, Ward-Caviness CK, Tsai PC, et al. DNA methylation-based measures of biological age: meta-analysis predicting time to death. *Aging (Albany NY).* 2016;8(9):1844-65.

32. Wang D, Hu B, Hu C, Zhu F, Liu X, Zhang J, et al. Clinical Characteristics of 138 Hospitalized Patients With 2019 Novel Coronavirus-Infected Pneumonia in Wuhan, China. *JAMA.* 2020;323(11):1061-9.

33. Toapanta FR, and Ross TM. Impaired immune responses in the lungs of aged mice following influenza infection. *Respir Res.* 2009;10(1):112.

34. Boothby IC, Cohen JN, and Rosenblum MD. Regulatory T cells in skin injury: At the crossroads of tolerance and tissue repair. *Sci Immunol.* 2020;5(47):eaaz9631.

35. Dial CF, Tune MK, Doerschuk CM, and Mock JR. Foxp3(+) Regulatory T Cell Expression of Keratinocyte Growth Factor Enhances Lung Epithelial Proliferation. *Am J Respir Cell Mol Biol.* 2017;57(2):162-73.

36. Kuswanto W, Burzyn D, Panduro M, Wang KK, Jang YC, Wagers AJ, et al. Poor Repair of Skeletal Muscle in Aging Mice Reflects a Defect in Local, Interleukin-33-Dependent Accumulation of Regulatory T Cells. *Immunity.* 2016;44(2):355-67.

37. Ohkura N, Yasumizu Y, Kitagawa Y, Tanaka A, Nakamura Y, Motooka D, et al. Regulatory T Cell-Specific Epigenomic Region Variants Are a Key Determinant of Susceptibility to Common Autoimmune Diseases. *Immunity.* 2020.

38. Morales-Nebreda L, Helmin KA, and Singer BD. CoRESTed development of regulatory T cells. *The Journal of Clinical Investigation.* 2020;130(4):1618-21.

39. Morales-Nebreda L, Chi M, Lecuona E, Chandel NS, Dada LA, Ridge K, et al. Intratracheal administration of influenza virus is superior to intranasal administration as a model of acute lung injury. *Journal of virological methods.* 2014;209:116-20.

40. Singer BD, Mock JR, D'Alessio FR, Aggarwal NR, Mandke P, Johnston L, et al. Flow-cytometric method for simultaneous analysis of mouse lung epithelial, endothelial, and hematopoietic lineage cells. *American journal of physiology Lung cellular and molecular physiology.* 2016;310(9):L796-801.

41. Tighe RM, Redente EF, Yu YR, Herold S, Sperling AI, Curtis JL, et al. Improving the Quality and Reproducibility of Flow Cytometry in the Lung. An Official American Thoracic Society Workshop Report. *Am J Respir Cell Mol Biol.* 2019;61(2):150-61.

42. Weinberg SE, Singer BD, Steinert EM, Martinez CA, Mehta MM, Martínez-Reyes I, et al. Mitochondrial complex III is essential for suppressive function of regulatory T cells. *Nature.* 2019;565(7740):495-9.

43. McGrath-Morrow SA, Ndeh R, Helmin KA, Chen SY, Anekalla KR, Abdala-Valencia H, et al. DNA methylation regulates the neonatal CD4(+) T-cell response to pneumonia in mice. *J Biol Chem.* 2018;293(30):11772-83.

44. Subramanian A, Tamayo P, Mootha VK, Mukherjee S, Ebert BL, Gillette MA, et al. Gene set enrichment analysis: A knowledge-based approach for interpreting genome-wide expression profiles. *Proceedings of the National Academy of Sciences.* 2005;102(43):15545.

45. Singer BD. A Practical Guide to the Measurement and Analysis of DNA Methylation. *Am J Respir Cell Mol Biol.* 2019;61(4):417-28.

46. Wang L, Ozark PA, Smith ER, Zhao Z, Marshall SA, Rendleman EJ, et al. TET2 coactivates gene expression through demethylation of enhancers. *Sci Adv.* 2018;4(11):eaau6986.

47. Piunti A, Smith ER, Morgan MAJ, Ugarenko M, Khaltyan N, Helmin KA, et al. CATACOMB: An endogenous inducible gene that antagonizes H3K27 methylation activity of Polycomb repressive complex 2 via an H3K27M-like mechanism. *Sci Adv.* 2019;5(7):eaax2887.

48. Workman CJ, Collison LW, Bettini M, Pillai MR, Rehg JE, and Vignali DA. In vivo Treg suppression assays. *Methods Mol Biol.* 2011;707:119-56.

49. Radigan KA, Morales-Nebreda L, Soberanes S, Nicholson T, Nigdelioglu R, Cho T, et al. Impaired clearance of influenza A virus in obese, leptin receptor deficient mice is independent of leptin signaling in the lung epithelium and macrophages. *PloS one.* 2014;9(9):e108138.

Figures

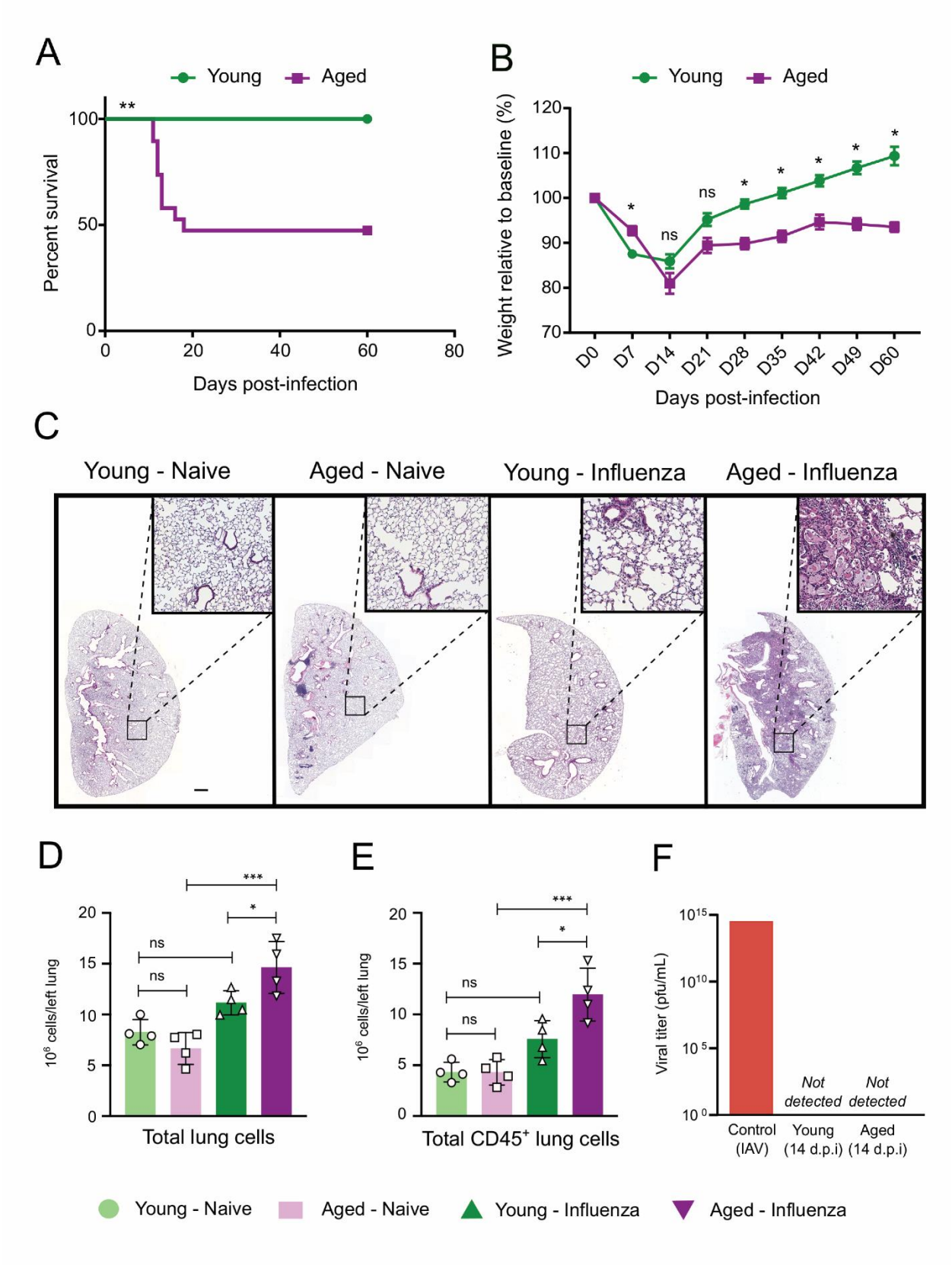
A
Young
Aged
**
100
50
0
Percent survival
0
20
40
60
80
Days post-infection
B
Young
Aged
Weight relative to baseline (%)
120
110
100
90
80
70
*
ns
ns
*
*
*
*
D0
D7
D14
D21
D28
D35
D42
D49
D60
Days post-infection
C
Young - Naive
Aged - Naive
Young - Influenza
Aged - Influenza
D
***
*
ns
ns
20
15
10
5
0
10^6 cells/left lung
Total lung cells
E
***
*
ns
ns
20
15
10
5
0
10^6 cells/left lung
Total CD45+ lung cells
F
10^15
10^10
10^5
10^0
Viral titer (pfu/mL)
Not detected
Not detected
Control (IAV)
Young (14 d.p.i)
Aged (14 d.p.i)
Young - Naive
Aged - Naive
Young - Influenza
Aged - Influenza

Figure 1. Aged mice demonstrate increased mortality and lung inflammation during recovery from influenza infection. (A) Survival curve comparison of young (2 months, *n* = 20) and aged (18 months, *n* = 19) wild-type mice using log-rank (Mantel-Cox) test. (B) Weight loss percentage from baseline in young (2-4 months, *n* = 20) and aged (18-22 months, *n* = 19) mice compared using a mixed-effects model (REML) with Sidak's *post-hoc* multiple comparisons test. Data presented as mean ± SEM. (C) Representative lung histopathology (hematoxylin-eosin staining) of young and aged mice during the naïve state and recovery phase following influenza infection (day 60). Original magnification x10, scale bar 500μm. (D) Flow cytometry quantitative analysis of total number of cells and (E) Total number of $CD45^+$ cells from left lung during the naïve state and recovery phase from influenza infection. (F) Viral titer measurement of lung homogenates in young and aged mice 14 days post-infection (d.p.i). Positive control from influenza A/WSN/33 (H1N1) viral stock. *n* = 4 mice/group (young - influenza and aged - influenza). Data presented as mean ± SD, one-way ANOVA with Holm-Sidak's *post-hoc* testing for multiple comparisons (D and E). *** $p < 0.0005$, ** $p < 0.005$, * $p < 0.05$, ns = not significant. *n* = 4 mice/group (young – naïve, aged – naïve, young – influenza and aged – influenza) for figures D and E.

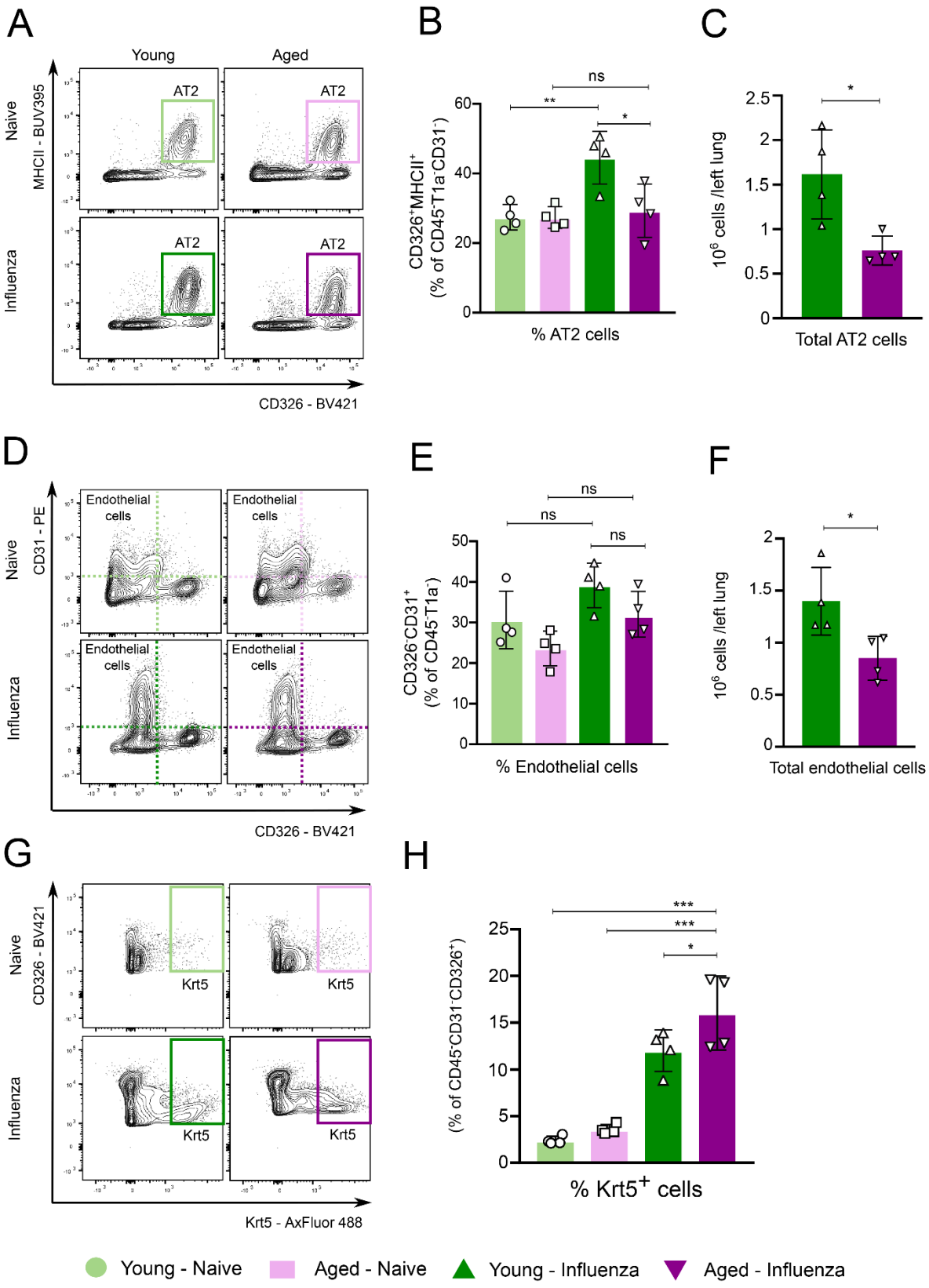
A
Young
Aged
Naive
Influenza
MHCII - BUV395
AT2
CD326 - BV421
B
ns
**
*
CD326+MHCII+ (% of CD45-T1a-CD31-)
% AT2 cells
C
*
10^6 cells /left lung
Total AT2 cells
D
Naive
Influenza
CD31 - PE
Endothelial cells
CD326 - BV421
E
ns
ns
ns
CD326-CD31+ (% of CD45-T1a-)
% Endothelial cells
F
*
10^6 cells /left lung
Total endothelial cells
G
Naive
Influenza
CD326 - BV421
Krt5
Krt5 - AxFluor 488
H
***
***
*
(% of CD45-CD31-CD326+)
% Krt5+ cells
Young - Naive
Aged - Naive
Young - Influenza
Aged - Influenza

Figure 2. Aging results in failure to repopulate the alveolar epithelial-capillary barrier during recovery 60 days post-influenza infection. (A) Representative flow cytometry contour plot analysis of type II alveolar epithelial cells (AT2). See Supplemental Figure 2 for parent gating. (B) $CD326^+$ $MHCII^+$ type II alveolar epithelial cells as a percentage of $CD45^-$ $T1\alpha^-$ $CD31^-$ cells. (C) Total type II alveolar epithelial cells from left lung. (D) Representative flow cytometry contour plot analysis of endothelial cells. (E) $CD326^-$ $CD31^+$ endothelial cells as a percentage of $CD45^-$ $T1\alpha^-$ cells. (F) Total endothelial cells from left lung. (G) Representative flow cytometry contour plot analysis of $Krt5^+$ cells. (H) $Krt5^+$ epithelial cells as a percentage of $CD45^-$ $CD31^-$ $CD326^+$ cells. Data presented as mean ± SD, one-way ANOVA with Holm-Sidak's *post-hoc* testing for multiple comparisons (B, E and H) or Mann Whitney test (C and F). *** $p < 0.0005$, ** $p < 0.005$, * $p < 0.05$, ns = not significant. $n = 4$ mice/group (young – naïve, aged – naïve, young – influenza and aged – influenza) for all figures.

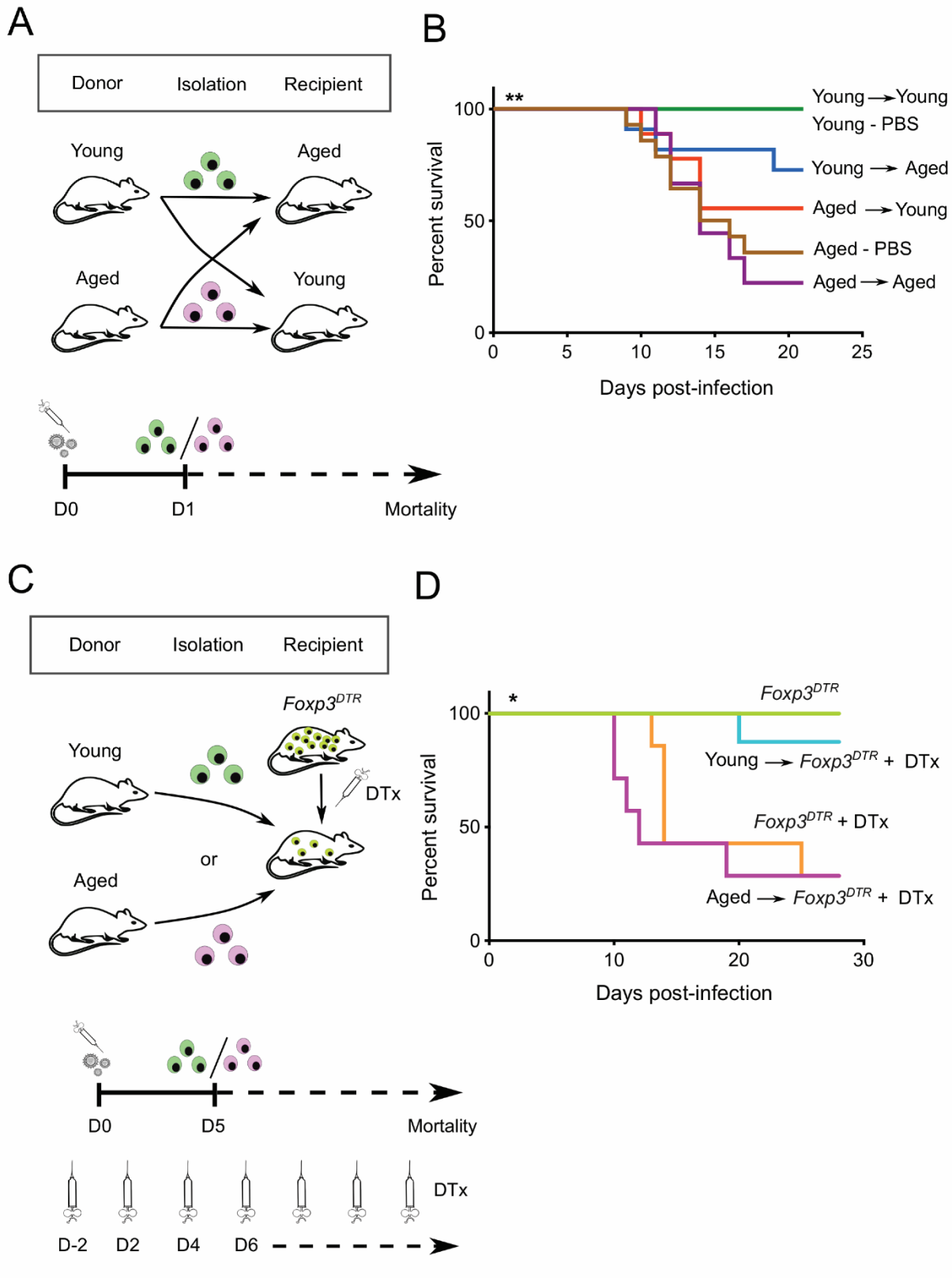
A
Donor
Isolation
Recipient
Young
Aged
Aged
Young
D0
D1
Mortality
B
**
Young → Young
Young - PBS
Young → Aged
Aged → Young
Aged - PBS
Aged → Aged
Percent survival
Days post-infection
C
Donor
Isolation
Recipient
Foxp3DTR
Young
DTx
or
Aged
D0
D5
Mortality
DTx
D-2
D2
D4
D6
D
*
Foxp3DTR
Young → Foxp3DTR + DTx
Foxp3DTR + DTx
Aged → Foxp3DTR + DTx
Percent survival
Days post-infection

Figure 3. Age determines the tissue protective phenotype of Treg cells during influenza-induced lung injury. (A) Schematic of experimental design. (B) Survival curve of adoptive Treg cell transfer experiments. *n* = 5 (Young – PBS), 14 (Aged – PBS), 9 (Young into Young), 9 (Aged into Aged), 9 (Aged into Young) and 11 (Young into Aged) animals per group. (C) Schematic of experimental design. (D) Survival curve of adoptive Treg cell transfer experiments in *Foxp3*^{DTR} mice. *n* = 7-8 animals per group except for the *Foxp3*^{DTR} group (*n* = 3). DTx denotes diphtheria toxin. Survival curves of mice compared using log-rank (Mantel-Cox) test. ** $p < 0.005$ and * $p < 0.05$.

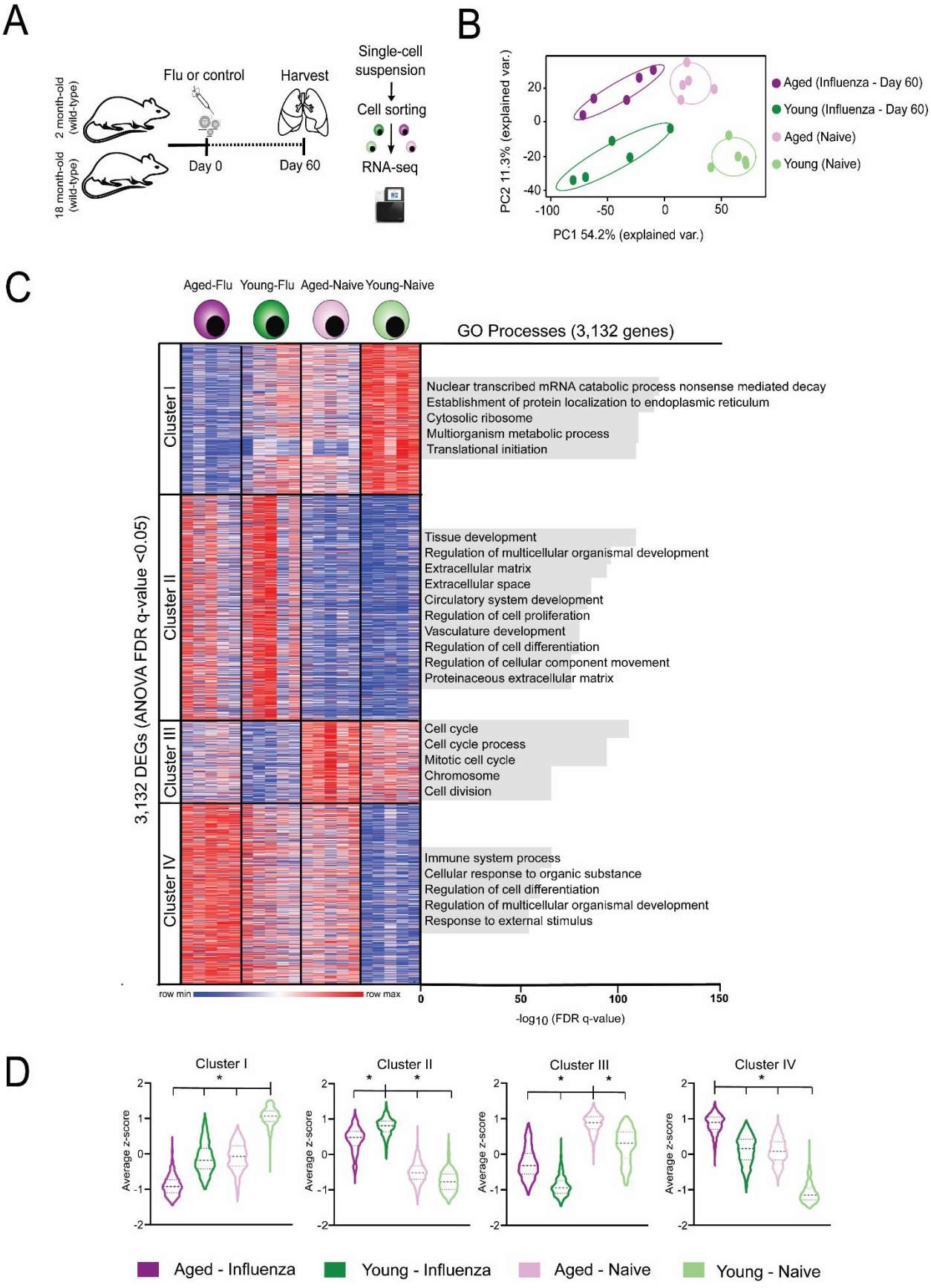
A
2 month-old (wild-type)
18 month-old (wild-type)
Flu or control
Harvest
Day 0
Day 60
Single-cell suspension
Cell sorting
RNA-seq
B
PC2 11.3% (explained var.)
PC1 54.2% (explained var.)
Aged (Influenza - Day 60)
Young (Influenza - Day 60)
Aged (Naive)
Young (Naive)
C
Aged-Flu
Young-Flu
Aged-Naive
Young-Naive
GO Processes (3,132 genes)
3,132 DEGs (ANOVA FDR q-value <0.05)
Cluster I
Cluster II
Cluster III
Cluster IV
Nuclear transcribed mRNA catabolic process nonsense mediated decay
Establishment of protein localization to endoplasmic reticulum
Cytosolic ribosome
Multiorganism metabolic process
Translational initiation
Tissue development
Regulation of multicellular organismal development
Extracellular matrix
Extracellular space
Circulatory system development
Regulation of cell proliferation
Vasculature development
Regulation of cell differentiation
Regulation of cellular component movement
Proteinaceous extracellular matrix
Cell cycle
Cell cycle process
Mitotic cell cycle
Chromosome
Cell division
Immune system process
Cellular response to organic substance
Regulation of cell differentiation
Regulation of multicellular organismal development
Response to external stimulus
row min
row max
-log10 (FDR q-value)
D
Cluster I
Cluster II
Cluster III
Cluster IV
Average z-score
Aged - Influenza
Young - Influenza
Aged - Naive
Young - Naive

Figure 4. Young and aged Treg cells differ in their transcriptional response during recovery from influenza infection. (A) Schematic of experimental design. (B) Principal component analysis of 3,132 differentially expressed genes identified from a generalized linear model and ANOVA-like testing with FDR *q*-value < 0.05. Ellipses represent normal contour lines with one standard deviation probability. (C) *K*-means clustering of 3,132 genes with an FDR *q*-value < 0.05 comparing the cell populations from (B) with $k = 4$ and scaled as *z*-scores across rows. Top five gene ontology (GO) processes derived from clusters I, III and IV, and top 10 GO processes derived from cluster II are annotated and ranked by $-\log_{10}$-transformed FDR *q*-value. (D) Average *z*-scores for the four clusters shown in (C). Violin plots show median and quartiles. One-way ANOVA with two-stage linear step-up procedure of Benjamini, Krieger and Yekutieli with $Q = 5\%$. * $q < 0.05$. $n = 5$ mice/group (young – naïve, aged – naïve, young – influenza and aged – influenza) for all figures.

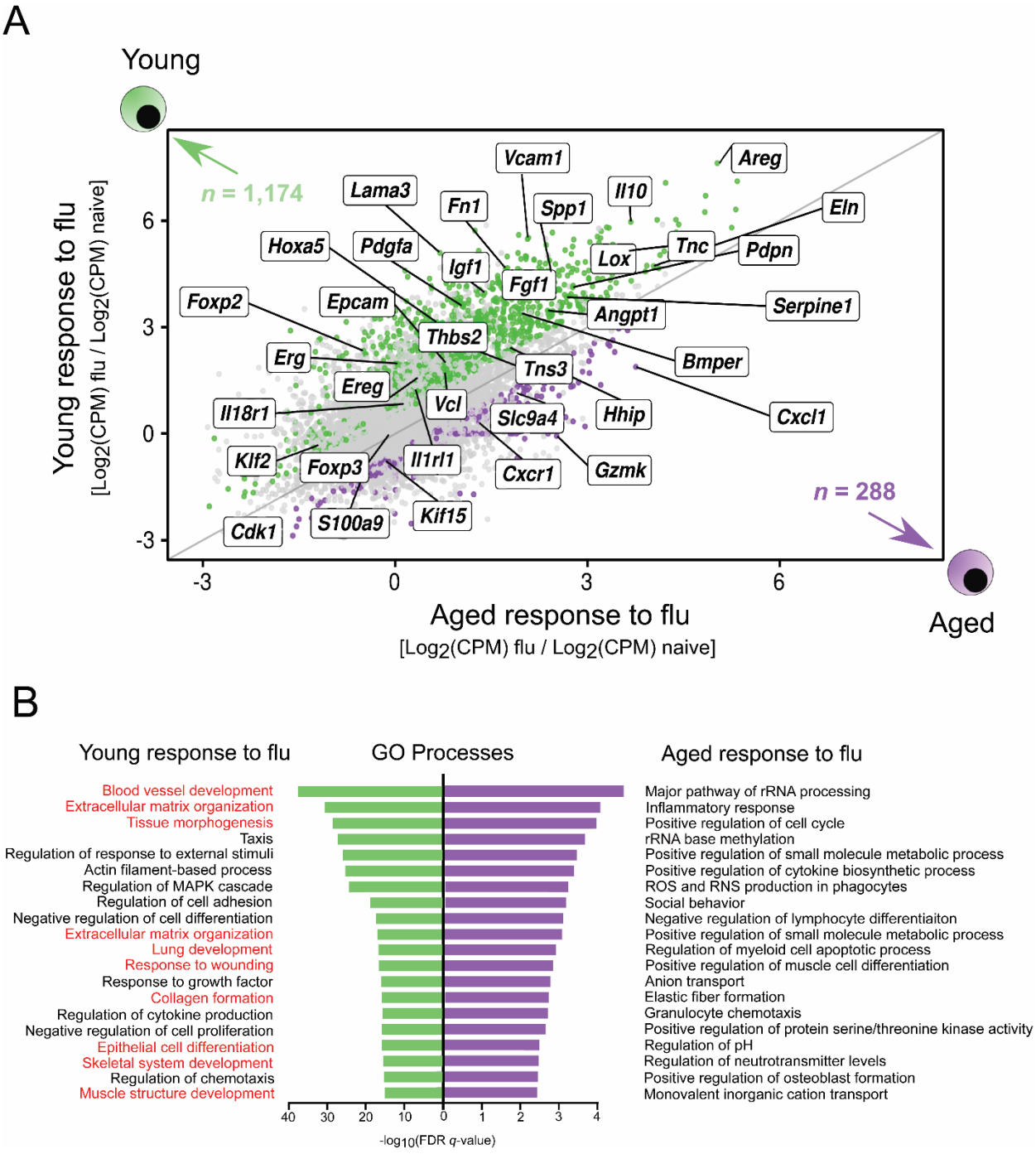
A
Young
n = 1,174
Vcam1
Areg
Lama3
Il10
Fn1
Spp1
Eln
Hoxa5
Pdgfa
Tnc
Pdpn
Igf1
Lox
Fgf1
Foxp2
Epcam
Angpt1
Serpine1
Thbs2
Erg
Tns3
Bmper
Ereg
Vcl
Il18r1
Slc9a4
Hhip
Cxcl1
Klf2
Foxp3
Il1rl1
Cxcr1
Gzmk
n = 288
Cdk1
S100a9
Kif15
Young response to flu
[Log2(CPM) flu / Log2(CPM) naive]
Aged response to flu
[Log2(CPM) flu / Log2(CPM) naive]
Aged
B
Young response to flu
GO Processes
Aged response to flu
Blood vessel development
Extracellular matrix organization
Tissue morphogenesis
Taxis
Regulation of response to external stimuli
Actin filament-based process
Regulation of MAPK cascade
Regulation of cell adhesion
Negative regulation of cell differentiation
Extracellular matrix organization
Lung development
Response to wounding
Response to growth factor
Collagen formation
Regulation of cytokine production
Negative regulation of cell proliferation
Epithelial cell differentiation
Skeletal system development
Regulation of chemotaxis
Muscle structure development
Major pathway of rRNA processing
Inflammatory response
Positive regulation of cell cycle
rRNA base methylation
Positive regulation of small molecule metabolic process
Positive regulation of cytokine biosynthetic process
ROS and RNS production in phagocytes
Social behavior
Negative regulation of lymphocyte differentiaiton
Positive regulation of small molecule metabolic process
Regulation of myeloid cell apoptotic process
Positive regulation of muscle cell differentiation
Anion transport
Elastic fiber formation
Granulocyte chemotaxis
Positive regulation of protein serine/threonine kinase activity
Regulation of pH
Regulation of neutrotransmitter levels
Positive regulation of osteoblast formation
Monovalent inorganic cation transport
-log10(FDR q-value)

Figure 5. Young Treg cells upregulate a pro-repair transcriptional program during recovery from influenza infection. (A) Fold-change-fold-change plot for the young Treg cell response to influenza infection versus the aged Treg cell response to influenza infection highlighting genes exhibiting $q < 0.05$ and fold-change (FC) > 0.5 (green dots = young and purple dots = aged). Numbers of differentially expressed genes are indicated. (B) Top 20 gene ontology (GO) processes derived from differentially expressed genes ($q < 0.05$) from (A) for young Treg cells (1,174 genes) and aged Treg cells (288 genes) are annotated and ranked by $-\log_{10}$-transformed FDR q-value. Red font denotes pro-repair processes in young Treg cells $n = 5$ mice/group (young – naïve, aged – naïve, young – influenza and aged – influenza) for all figures.

A

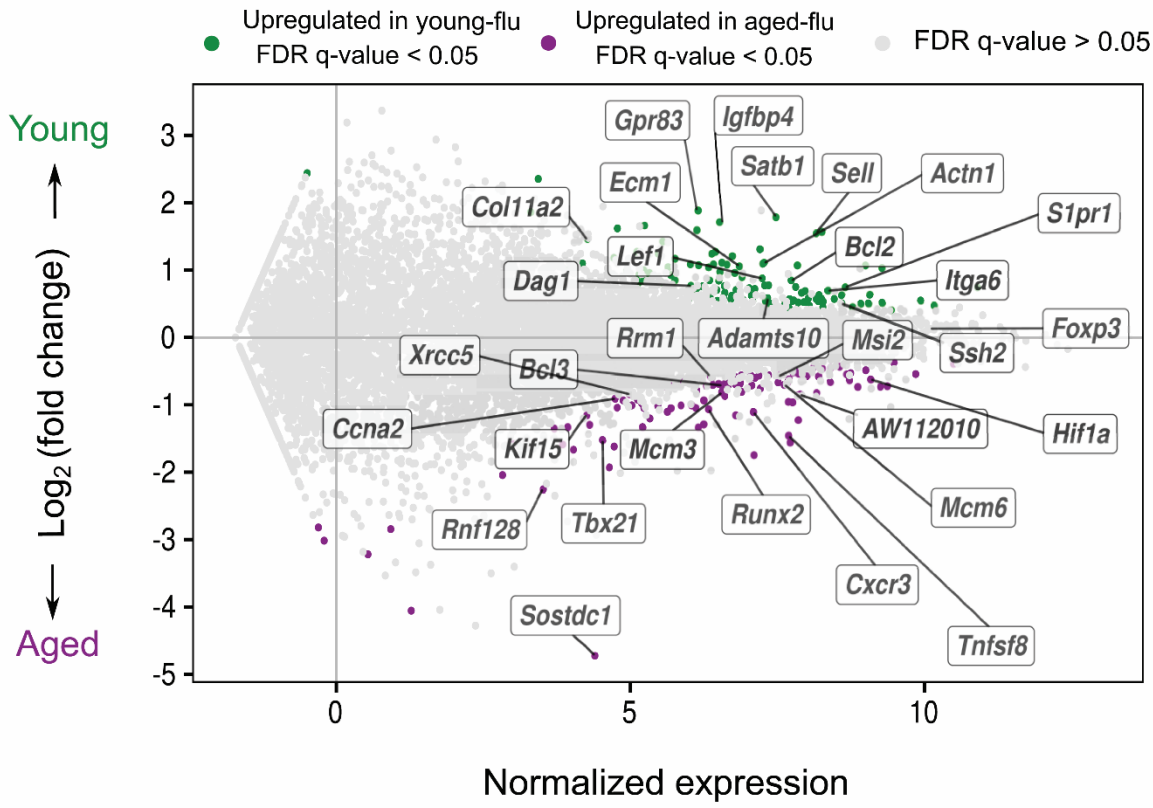

B

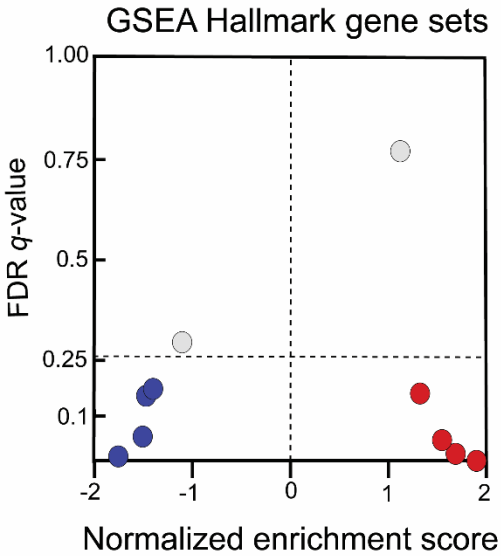

Rank	Hallmark	NES
1	E2F targets	1.83
2	G2M checkpoint	1.64
3	Myc targets	1.55
4	Allograft rejection	1.44
5	IL2 STAT5 signal	1.17

Rank	Hallmark	NES
1	EMT	-1.81
2	Myogenesis	-1.58
3	UV response DN	-1.44
4	Coagulation	-1.40
5	Angiogenesis	-1.33

Upregulated in Aged-Flu, FDR *q*-val <0.25

Downregulated in Aged-Flu, FDR *q*-val <0.25

Figure 6. Aged Treg cells downregulate pro-repair programs during recovery from influenza pneumonia when compared with young hosts. (A) MA plot comparing gene expression of young Treg versus aged Treg cells during the recovery phase from influenza infection. Genes of interest are annotated. (B) Gene set enrichment analysis (GSEA) dot plot highlighting key statistics (FDR *q*-value and normalized enrichment score or NES) and gene set enrichment per phenotype. Genes were ordered by $\log_2$(fold-change) and ranked by the aged Treg cell phenotype. Red dots denote gene sets with a positive enrichment score or enrichment at the top of the ranked list. Blue dots denote gene sets with a negative enrichment score or enrichment at the bottom of the ranked list. *n* = 5 mice/group (young – influenza and aged – influenza) for all figures.

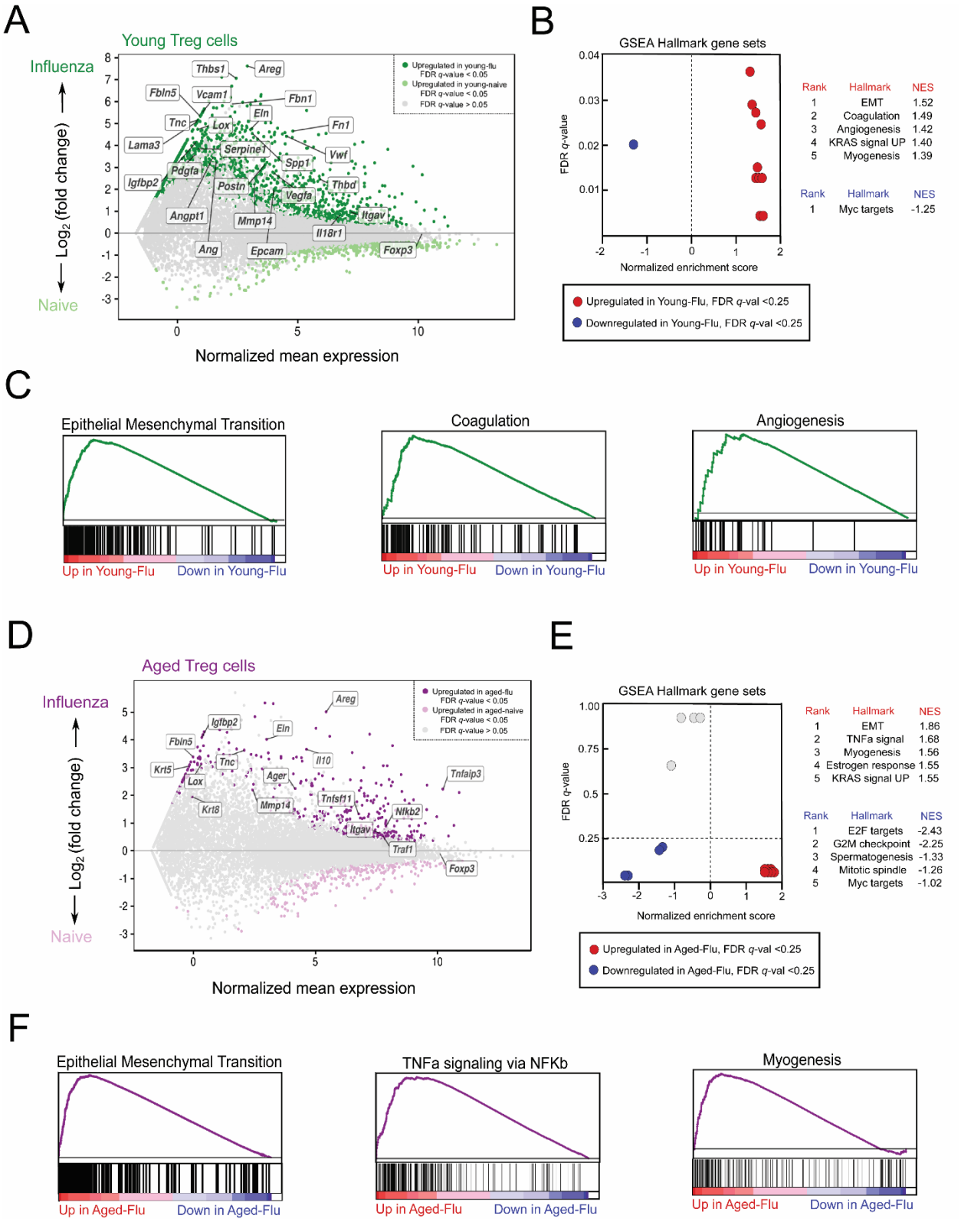
A
Young Treg cells
Influenza
Naive
Log2 (fold change)
Normalized mean expression
Upregulated in young-flu FDR q-value < 0.05
Upregulated in young-naive FDR q-value < 0.05
FDR q-value > 0.05
Thbs1
Areg
Fbln5
Vcam1
Fbn1
Eln
Tnc
Lox
Fn1
Lama3
Serpine1
Vwf
Pdgfa
Spp1
Igfbp2
Postn
Thbd
Vegfa
Angpt1
Mmp14
Itgav
Il18r1
Ang
Epcam
Foxp3
B
GSEA Hallmark gene sets
FDR q-value
Normalized enrichment score
Upregulated in Young-Flu, FDR q-val <0.25
Downregulated in Young-Flu, FDR q-val <0.25
Rank Hallmark NES
1 EMT 1.52
2 Coagulation 1.49
3 Angiogenesis 1.42
4 KRAS signal UP 1.40
5 Myogenesis 1.39
Rank Hallmark NES
1 Myc targets -1.25
C
Epithelial Mesenchymal Transition
Coagulation
Angiogenesis
Up in Young-Flu
Down in Young-Flu
D
Aged Treg cells
Influenza
Naive
Log2 (fold change)
Normalized mean expression
Upregulated in aged-flu FDR q-value < 0.05
Upregulated in aged-naive FDR q-value < 0.05
FDR q-value > 0.05
Areg
Igfbp2
Eln
Fbln5
Il10
Krt5
Tnc
Ager
Tnfaip3
Lox
Tnfsf11
Krt8
Mmp14
Nfkb2
Itgav
Traf1
Foxp3
E
GSEA Hallmark gene sets
FDR q-value
Normalized enrichment score
Upregulated in Aged-Flu, FDR q-val <0.25
Downregulated in Aged-Flu, FDR q-val <0.25
Rank Hallmark NES
1 EMT 1.86
2 TNFa signal 1.68
3 Myogenesis 1.56
4 Estrogen response 1.55
5 KRAS signal UP 1.55
Rank Hallmark NES
1 E2F targets -2.43
2 G2M checkpoint -2.25
3 Spermatogenesis -1.33
4 Mitotic spindle -1.26
5 Myc targets -1.02
F
Epithelial Mesenchymal Transition
TNFa signaling via NFKb
Myogenesis
Up in Aged-Flu
Down in Aged-Flu

Figure 7. Aged lung Treg cells fail to upregulate a pro-repair transcriptional program to the same extent as young Treg cells during recovery from influenza infection. (A) MA plot comparing gene expression of young Treg cells during the naïve state with young Treg cells during the recovery phase of influenza infection. Genes of interest are annotated and *y*-axis denotes fold-change dynamic range. (B) MA plot comparing gene expression of aged Treg cells during the naïve state with aged Treg cells during the recovery phase of influenza infection. Genes of interest are annotated and *y*-axis denotes fold-change dynamic range. Note that the y-axis extends to +8 in (A) and +5 in (B). (C) and (D) GSEA dot plot results highlighting key statistics (FDR *q*-value and normalized enrichment score or NES) and enriched gene sets per phenotype. Genes were ordered by $\log_2$(fold-change) and ranked by the young Treg cell-influenza (C) or aged Treg cell-influenza (D) phenotype. Red dots denote gene sets with a positive enrichment score or enrichment at the top of the ranked list. Blue dots denote gene sets with a negative enrichment score or enrichment at the bottom of the ranked list. (E) and (F) highlight top three GSEA positive enrichment plots for the young Treg cell-influenza (E) or aged Treg cell-influenza (F) phenotype. *n* = 5 mice/group (young – naïve, aged – naïve, young – influenza and aged – influenza) for all figures.

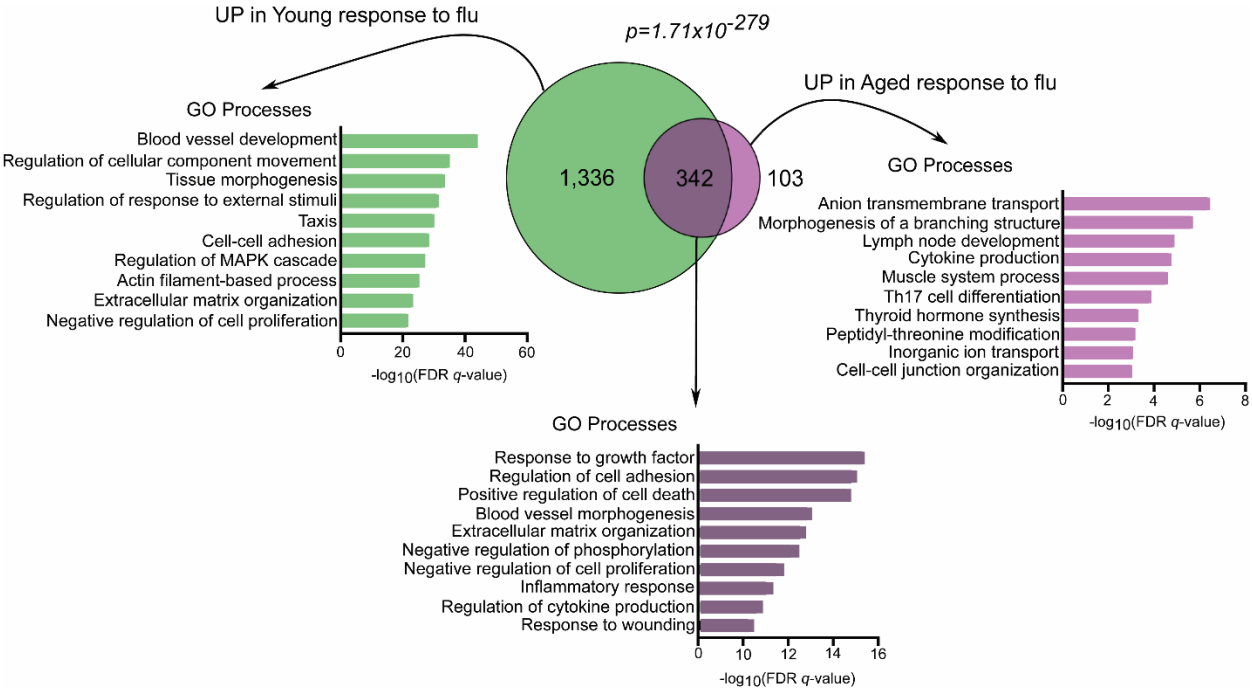
UP in Young response to flu
p=1.71x10-279
UP in Aged response to flu
1,336
342
103
GO Processes
Blood vessel development
Regulation of cellular component movement
Tissue morphogenesis
Regulation of response to external stimuli
Taxis
Cell-cell adhesion
Regulation of MAPK cascade
Actin filament-based process
Extracellular matrix organization
Negative regulation of cell proliferation
0 20 40 60
-log10(FDR q-value)
GO Processes
Anion transmembrane transport
Morphogenesis of a branching structure
Lymph node development
Cytokine production
Muscle system process
Th17 cell differentiation
Thyroid hormone synthesis
Peptidyl-threonine modification
Inorganic ion transport
Cell-cell junction organization
0 2 4 6 8
-log10(FDR q-value)
GO Processes
Response to growth factor
Regulation of cell adhesion
Positive regulation of cell death
Blood vessel morphogenesis
Extracellular matrix organization
Negative regulation of phosphorylation
Negative regulation of cell proliferation
Inflammatory response
Regulation of cytokine production
Response to wounding
0 10 12 14 16
-log10(FDR q-value)

Figure 8. Comparison of enriched gene ontology processes during recovery from influenza pneumonia in young and aged Treg cells. Venn diagram partitioning into upregulated genes in young Treg cells during recovery from influenza infection (green, 1,336 genes), upregulated genes in aged Treg cells during recovery from influenza infection (light purple, 103 genes) and upregulated genes in both young and aged Treg cells during recovery from influenza infection (dark purple intersection, 342 genes). FDR *q*-value < 0.05. A hypergeometric *p*-value is shown. Top 10 gene ontology (GO) processes derived from genes in each partition of the Venn diagram are annotated and ranked by $-\log_{10}$-transformed FDR *q*-value. *n* = 5 mice/group (young – influenza and aged – influenza).

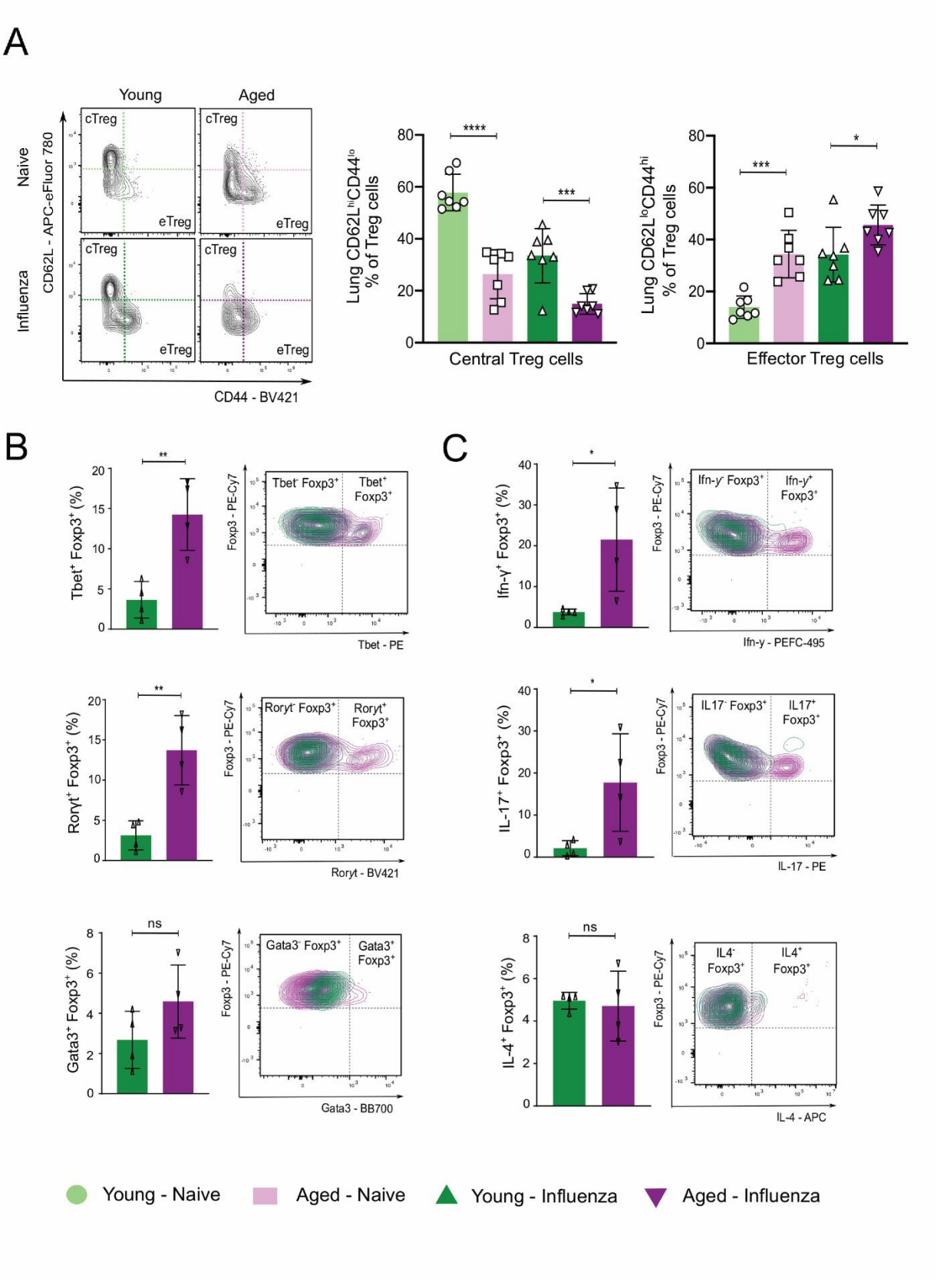
A
Young
Aged
Naive
Influenza
CD62L - APC-eFluor 780
CD44 - BV421
cTreg
eTreg
Lung CD62L^hiCD44^lo % of Treg cells
Central Treg cells
Lung CD62L^loCD44^hi % of Treg cells
Effector Treg cells
B
Tbet+ Foxp3+ (%)
Tbet- Foxp3+
Tbet+ Foxp3+
Foxp3 - PE-Cy7
Tbet - PE
Rorγt+ Foxp3+ (%)
Rorγt- Foxp3+
Rorγt+ Foxp3+
Rorγt - BV421
Gata3+ Foxp3+ (%)
Gata3- Foxp3+
Gata3+ Foxp3+
Gata3 - BB700
ns
C
Ifn-γ+ Foxp3+ (%)
Ifn-γ- Foxp3+
Ifn-γ+ Foxp3+
Ifn-γ - PEFC-495
IL-17+ Foxp3+ (%)
IL17- Foxp3+
IL17+ Foxp3+
IL-17 - PE
IL-4+ Foxp3+ (%)
IL4- Foxp3+
IL4+ Foxp3+
IL-4 - APC
Young - Naive
Aged - Naive
Young - Influenza
Aged - Influenza

Figure 9. Aging results in induction of a Treg cell pro-inflammatory phenotype following recovery from influenza infection. (A) Representative flow cytometry contour plot analysis of central Treg (cTreg) cells and effector Treg (eTreg) cells. Percentage of lung cTreg cells ($CD62L^{hi}CD44^{lo}$) and lung eTreg cells ($CD62L^{lo}CD44^{hi}$) of lung Treg cells. n = 7 mice/group (young – naïve, aged – naïve, young – influenza and aged – influenza) (B) Representative contour plots and pairwise comparison of percentage (%) of $CD4^{+}Foxp3^{+}$ cells expressing T helper cell canonical transcription factors. (C) Representative contour plots and pairwise comparison of percentage (%) of $CD4^{+}Foxp3^{+}$ cells expressing pro-inflammatory cytokines. Data presented as mean ± SD, one-way ANOVA with Holm-Sidak's *post-hoc* testing for multiple comparisons (A) or Mann Whitney test (B and C). **** $p < 0.0001$, *** $p < 0.0005$, ** $p < 0.005$, * $p < 0.05$, ns = not significant. n = 4 mice/group (young – influenza and aged – influenza) for figures B and C.

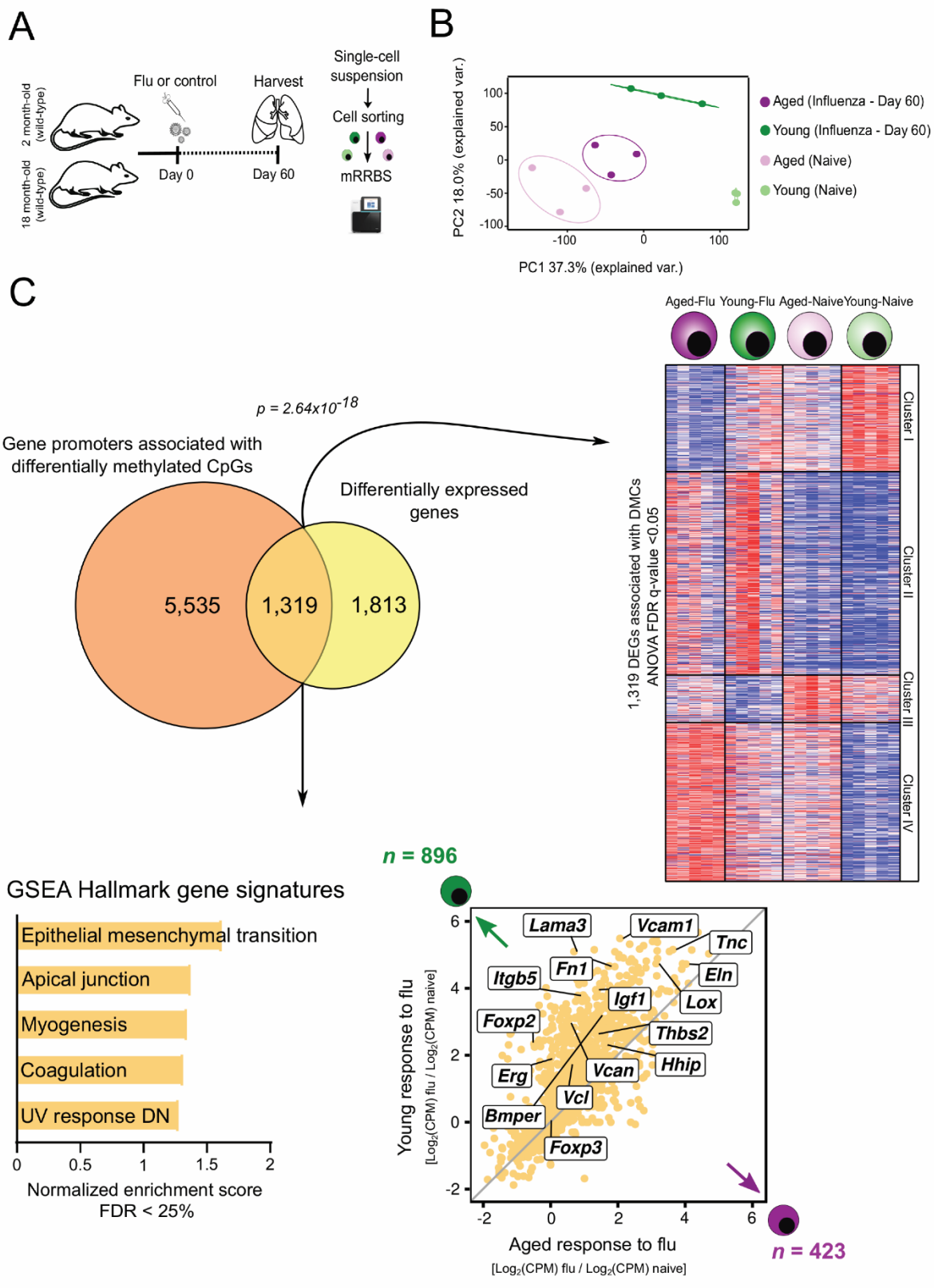
A
2 month-old (wild-type)
18 month-old (wild-type)
Flu or control
Day 0
Harvest
Day 60
Single-cell suspension
Cell sorting
mRRBS
B
PC2 18.0% (explained var.)
PC1 37.3% (explained var.)
Aged (Influenza - Day 60)
Young (Influenza - Day 60)
Aged (Naive)
Young (Naive)
C
Aged-Flu
Young-Flu
Aged-Naive
Young-Naive
p = 2.64x10-18
Gene promoters associated with differentially methylated CpGs
Differentially expressed genes
5,535
1,319
1,813
1,319 DEGs associated with DMCs
ANOVA FDR q-value <0.05
Cluster I
Cluster II
Cluster III
Cluster IV
GSEA Hallmark gene signatures
Epithelial mesenchymal transition
Apical junction
Myogenesis
Coagulation
UV response DN
Normalized enrichment score
FDR < 25%
n = 896
n = 423
Young response to flu
[Log2(CPM) flu / Log2(CPM) naive]
Aged response to flu
[Log2(CPM) flu / Log2(CPM) naive]
Lama3
Vcam1
Tnc
Fn1
Itgb5
Eln
Igf1
Lox
Foxp2
Thbs2
Hhip
Erg
Vcan
Vcl
Bmper
Foxp3

Figure 10. DNA methylation regulates the age-related pro-repair gene signature during recovery from influenza infection. (A) Schematic of experimental design. (B) Principal component analysis of ~70,000 differentially methylated cytosines (DMCs) identified from a generalized linear model and ANOVA-like testing with FDR *q*-value < 0.05. Ellipses represent normal contour lines with one standard deviation probability. *n* = 3 mice/group (young – naïve, aged – naïve, young – influenza and aged – influenza) (C) Venn diagram partitioning into differentially expressed genes or DEGs (yellow, 1,813 genes), gene promoters containing DMCs (dark orange, 5,535 genes) and genes which are both DEGs and have gene promoters containing DMCs (light orange intersection, 1,319 genes). Promoters were defined as 1 kb surrounding the transcription start site. A hypergeometric *p*-value is shown. *K*-means clustering of 1,319 genes with an FDR *q*-value < 0.05. Fold-change-fold-change plot for young Treg cell response to influenza versus aged Treg cell response to influenza infection highlighting methylation-regulated differentially expressed genes. GSEA results showing the top five positively enriched gene sets with an FDR *q*-value < 0.25. Genes were ordered by $\log_2$(fold-change) and ranked by the young Treg cell phenotype. *n* = 5 mice/group (young – naïve, aged – naïve, young – influenza and aged – influenza).